electronics

Article

IoT and Machine Learning for Crop Stress Assessment and Decision Support

Vesna Antoska Knights * and Vezirka Jankuloska

Faculty of Technology and Technical Sciences, University "St. Kliment Ohridski"—Bitola, Dimitar Vlahov 57, 1400 Veles, North Macedonia; vezirka.jankuloska@uklo.edu.mk
* Correspondence: vesna.knights@uklo.edu.mk

Abstract

Precision agriculture increasingly requires intelligent systems capable of integrating multimodal sensing with transparent decision support to enable timely and reliable crop management. This study proposes a hybrid intelligent IoT framework integrating environmental monitoring, wearable plant physiological sensing, AI-based pest-monitoring, machine-learning-based prediction of crop physiological stress, and explainable fuzzy rule-based decision support into a unified architecture for crop stress assessment. A novel Physiological Stress Index (PSI) was developed by combining vapor pressure deficit, relative humidity, Delta-T, leaf capacitance, and relative irradiance to provide an interpretable indicator of crop physiological stress. The proposed framework was experimentally validated under real field conditions using a commercial environmental monitoring station, wearable leaf sensors, AI-enabled pest-monitoring devices, and cloud-based analytics. Correlation analysis confirmed strong relationships between PSI and the principal environmental variables (VPD: $r = 0.980$, Delta-T: $r = 0.990$, RH: $r = -0.961$), demonstrating the internal consistency and sensitivity of the proposed index. At the 15 min forecasting horizon, Linear Regression and Gradient Boosting demonstrated virtually identical performance: Gradient Boosting achieved a marginally lower RMSE and higher R^2 (RMSE = 0.0273; $R^2 = 0.9810$), whereas Linear Regression achieved a slightly lower MAE (MAE = 0.0186). At the 1 h forecasting horizon, Gradient Boosting achieved the strongest performance ($R^2 = 0.9034$), indicating increasing relevance of nonlinear modelling at longer prediction horizons. The proposed framework demonstrates the feasibility of combining multimodal sensing, machine learning, explainable artificial intelligence, and edge-enabled IoT technologies to support proactive, transparent, and intelligent precision agriculture.

Keywords: Internet of Things; machine learning; multimodal sensing; crop stress assessment; physiological stress index; decision support system

Academic Editor: Domenico Ursino

Received: 22 July 2026
Revised: 20 August 2026
Accepted: 21 August 2026
Published: 25 August 2026

1. Introduction

Precision agriculture has emerged as a key technological approach for improving agricultural productivity, sustainability, and resource-use efficiency through the integration of advanced sensing technologies, embedded electronics, Internet of Things (IoT) infrastructures, wireless communication, edge computing, and cloud-based platforms [1,2]. These technologies enable continuous environmental monitoring, real-time data acquisition, and intelligent agricultural management, supporting irrigation scheduling, crop protection, and optimized resource utilization. Recent review studies have further emphasized that the integration of IoT, machine learning, edge computing, and intelligent sensing technologies is driving the next generation of precision agriculture systems [3–5]. Consequently, modern precision agriculture is evolving toward integrated edge-centric ecosystems that combine sensing, embedded processing, wireless communication, cloud-assisted analytics, and intelligent machine-learning models into unified agricultural monitoring frameworks [6–12].

Environmental monitoring represents a fundamental component of precision agriculture by continuously measuring climatic and microclimatic variables such as air temperature, relative humidity, precipitation, dew point, vapor pressure deficit (VPD), and Delta-T [13–15]. Furthermore, recent studies have highlighted the increasing importance of AI-assisted crop stress assessment and multimodal sensing for precision agriculture [5]. These measurements support irrigation scheduling, disease forecasting, and environmental risk assessment through distributed sensing platforms and cloud-based analytics. However, although environmental sensing accurately characterizes atmospheric conditions, it does not necessarily reflect the physiological status or stress response of crops. Consequently, relying solely on environmental measurements may limit agricultural decision making under dynamic field conditions where plant responses depend on species, developmental stage, and local microclimate [8,16–20].

To overcome these limitations, increasing attention has been directed toward wearable and plant-based sensing technologies capable of continuously monitoring physiological responses under real field conditions. Recent advances in non-destructive physiological sensing enable direct assessment of crop water status, transpiration dynamics, irradiance exposure, and stress responses before visible symptoms occur [14,21]. The integration of environmental and physiological measurements therefore provides complementary information for more comprehensive crop stress assessment and data-driven agricultural management [22–26].

In parallel, embedded artificial intelligence has become an important enabling technology for automated pest surveillance. AI-enabled smart traps equipped with imaging sensors, embedded processors, and wireless communication provide continuous insect detection and pest monitoring under field conditions, supporting early intervention while reducing manual inspections [27]. When integrated with environmental and physiological sensing, embedded AI contributes additional complementary information for intelligent crop monitoring within edge-enabled precision agriculture systems [28–33].

The growing availability of multimodal agricultural data requires decision-support systems capable of integrating heterogeneous sensing information into transparent and interpretable recommendations. Recent mathematical frameworks have further highlighted the importance of multimodal data fusion and uncertainty-aware decision making for improving the reliability of intelligent decision-support systems operating on heterogeneous sensing information [33]. In addition to predictive capability, modern agricultural decision-support systems should provide explainable recommendations that improve user confidence and facilitate the practical adoption of intelligent agricultural technologies [34–38]. Recent review studies have further emphasized that explainable artificial intelligence (XAI) is becoming an essential component of trustworthy smart agriculture by improving model transparency, interpretability, and user confidence [4,21].

Despite these advances, relatively few agricultural platforms integrate environmental sensing, physiological monitoring, embedded AI-based pest detection, wireless IoT communication, cloud synchronization, machine-learning based prediction, and explainable decision support within a unified edge-centric architecture suitable for real-time deployment. Most existing studies address these components separately, limiting interoperability, transparency, and practical applicability in precision agriculture [11,15,38].

Motivated by these challenges, this work presents a unified edge-centric multimodal agricultural intelligence framework integrating environmental sensing, wearable plant physiological monitoring, embedded AI-based pest surveillance, wireless IoT communication, cloud synchronization, machine learning-based prediction of the PSI, and explainable decision support. The proposed framework follows a hybrid intelligent architecture in which machine learning is employed for short-term prediction of the PSI, whereas transparent expert-defined rules generate interpretable agronomic recommendations based on the predicted PSI and pest-density information.

The main contributions of this work are as follows:

- A unified hybrid intelligent IoT framework integrating environmental sensing, wearable plant physiological monitoring, embedded AI-based pest surveillance, wireless IoT communication, cloud analytics, machine-learning prediction of crop physiological stress, and explainable rule-based decision support.
- A novel Physiological Stress Index (PSI) that combines environmental and physiological measurements into an interpretable indicator of crop physiological stress.
- An explainable rule-based decision-support model integrating the predicted Physiological Stress Index (PSI) with the normalized pest-density indicator to generate transparent and interpretable agronomic recommendations for short-term crop management.
- Experimental validation under real field conditions using commercial environmental monitoring stations, wearable plant sensors, AI-enabled pest-monitoring devices, machine-learning prediction, and cloud-based analytics, demonstrating the feasibility of the proposed framework for continuous precision agriculture monitoring.

2. Materials and Methods

2.1. Overall System Architecture

The proposed precision agriculture system was designed as an integrated edge-centric monitoring platform combining embedded environmental sensing, plant physiological monitoring, AI-based pest surveillance, wireless IoT communication, cloud-assisted analytics, and explainable decision support (Figure 1).

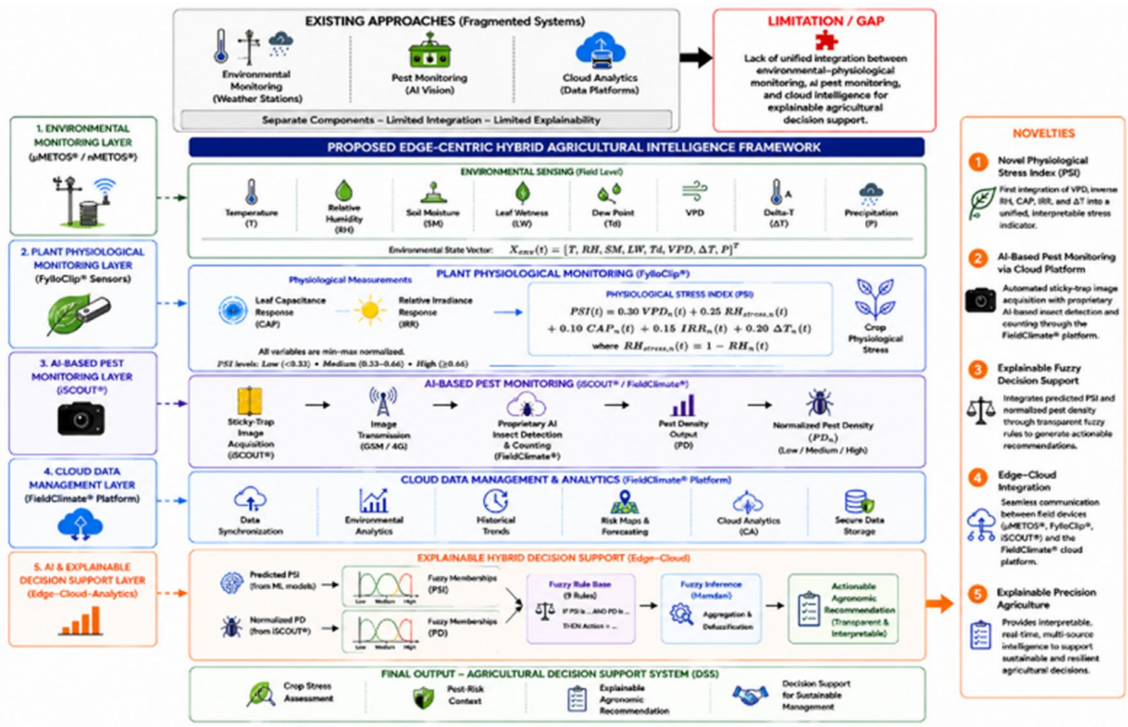

Figure 1. Proposed edge-centric hybrid framework for intelligent crop monitoring and explainable decision support.

The overall architecture consists of multiple interconnected subsystems that continuously acquire, transmit, process, and analyze multimodal agricultural data to support real-time crop monitoring and intelligent agricultural management. Figure 1 illustrates the overall hardware–software architecture of the proposed agricultural intelligence framework and the interactions between its principal functional components.

The experimental field is located in the Kumanovo region (Figure 2), North Macedonia (42.136837° N, 21.760454° E; elevation 424.7 m).

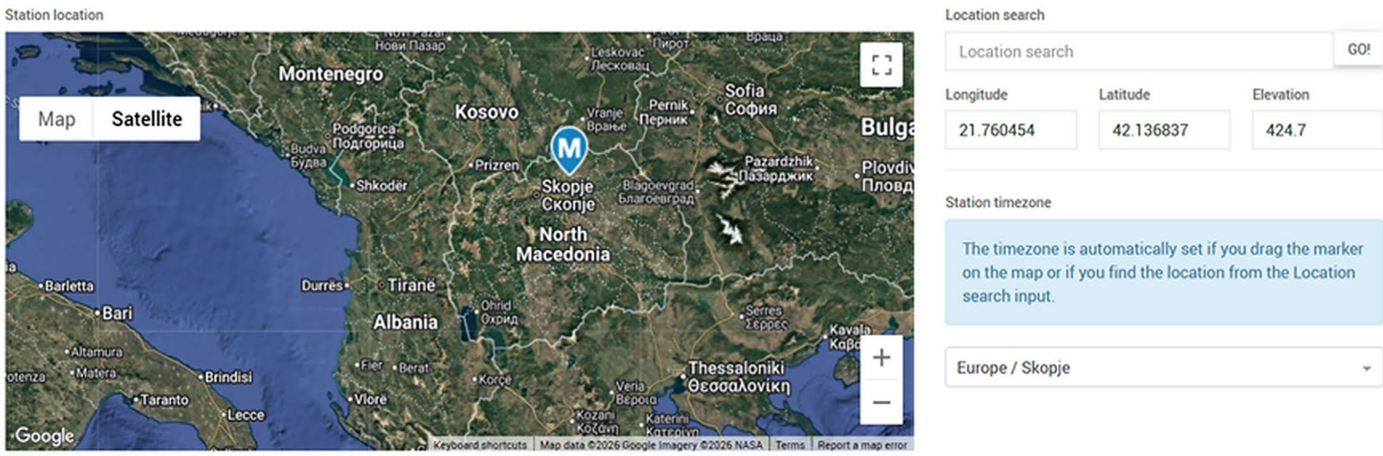

Figure 2. Location of the experimental field site in the Kumanovo region, North Macedonia (42.136837° N, 21.760454° E; elevation 424.7 m). Non-English text on the base map represents the local-script forms of geographic place names automatically displayed by Google Maps.

The field experiment was conducted on a local traditional Macedonian pepper (*Capsicum annuum* L.). At the beginning of physiological monitoring, the plants were in the vegetative growth stage, with developed leaves and no visible fruit formation. The crop was maintained under drip irrigation and routine field-management practices performed by the field operator. Two FylloClip sensors (Pessl Instruments, Weiz, Austria) were deployed on two separate pepper plants, with one sensor attached to one representative leaf of each plant. The field-monitoring dataset analyzed in this study covered the period from 21 May to 11 July 2026. Figure 3 presents the experimental deployment of the developed monitoring platform under real field conditions.

Environmental and physiological measurements were aligned according to their common timestamps. At each synchronized timestamp, capacitance measurements from the two FylloClip sensors were averaged to obtain a representative CAP value, while the corresponding irradiance measurements were averaged to obtain a representative IRR value. Thus, the two FylloClip sensors did not generate separate observations in the machine-learning dataset; each synchronized timestamp constituted a single temporal observation containing the environmental variables together with the averaged CAP and IRR values. Following timestamp alignment and data-quality filtering, the final dataset comprised 4893 synchronized temporal observations. These observations represent repeated temporal measurements and should not be interpreted as 4893 independent biological replicates.

The proposed framework consists of six interconnected functional subsystems responsible for environmental monitoring, plant physiological sensing, embedded AI pest surveillance, wireless communication, cloud analytics, and explainable decision support. Each subsystem is described in detail in the following sections.

(**a**) (**b**)

Figure 3. Experimental field deployment: (**a**) METOS STREMO environmental monitoring station; (**b**) autonomous wireless and solar-powered monitoring platform.

2.2. Environmental Monitoring Subsystem

The environmental monitoring subsystem constitutes the first sensing layer of the proposed agricultural intelligence framework and provides continuous atmospheric and microclimatic measurements under field conditions. The subsystem is based on distributed embedded sensing nodes equipped with meteorological sensors and low-power wireless communication modules for autonomous data acquisition and transmission.

As illustrated in Figure 4a–c, the environmental sensing unit integrates an embedded communication module together with sensor interface circuitry, and the field-deployed environmental monitoring station. The communication module provides wireless connectivity with the cloud platform, while the sensor interface enables acquisition of measurements from the connected field sensors.

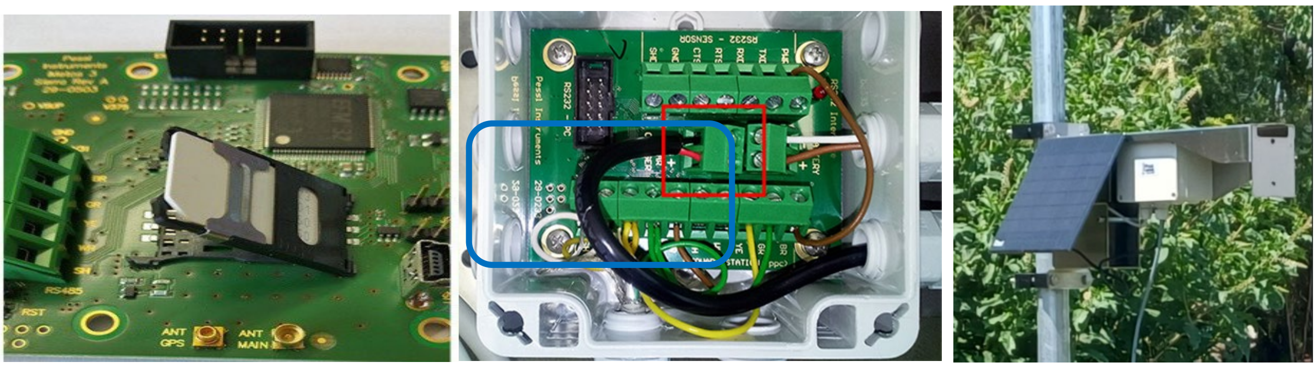

(**a**) (**b**) (**c**)

Figure 4. Environmental monitoring subsystem: (**a**) embedded communication module; (**b**) sensor interface; (**c**) environmental monitoring station deployed under field conditions.

The monitored variables include precipitation, air temperature, relative humidity, soil moisture, leaf wetness, dew point, vapor pressure deficit (VPD), and Delta-T. The corresponding environmental sensing vector is defined as

$$X_{env}(t) = [P(t), T(t), RH(t), SM(t), LW(t), DP(t), VPD(t), \Delta T(t)] \quad (1)$$

where

$P(t)$ is precipitation, $T(t)$ is air temperature, $RH(t)$ is relative humidity, $SM(t)$ denotes soil moisture; $LW(t)$ denotes leaf wetness; $DP(t)$ is dew point, $VPD(t)$ is vapor pressure deficit, and $\Delta T(t)$ is Delta-T.

These synchronized environmental measurements provide contextual information for subsequent physiological stress assessment and decision-support analysis.

2.3. Plant Physiological Monitoring Subsystem

The plant physiological monitoring subsystem represents the second sensing layer of the proposed agricultural intelligence framework. Unlike conventional environmental monitoring, which characterizes atmospheric conditions surrounding the crop, physiological sensing directly measures plant responses to environmental stimuli. This enables continuous assessment of crop water status, transpiration dynamics, and physiological stress, providing complementary information that cannot be obtained solely from meteorological observations.

The subsystem employs a non-destructive wearable sensing approach attached directly to plant leaves, enabling continuous monitoring under field conditions without affecting normal plant development. The physiological sensing platform combines capacitance-based measurements associated with leaf transpiration behavior and optical irradiance sensing for monitoring incident solar radiation influencing plant physiological activity. Figure 5 presents the physiological sensing device used for continuous monitoring of plant transpiration behavior and incident solar irradiance under field conditions.

(a) (b)

Figure 5. Physiological leaf sensor integrating capacitance-based transpiration sensing and photodiode irradiance monitoring: (**a**) FylloClip physiological leaf sensor; (**b**) sensor attached to a pepper leaf under field conditions.

The physiological sensing device combines capacitance-based transpiration sensing with photodiode irradiance measurements, enabling continuous monitoring of plant physiological responses under field conditions. The corresponding physiological sensing vector is defined in Table 1.

Table 1. Physiological variables acquired by sensor.

Variable	Symbol	Description	Role in the Proposed Framework
Leaf capacitance response	CAP	Indicator of plant transpiration and water status	Input to PSI
Relative irradiance	IRR	Indicator of incident solar radiation	Input to PSI

The two physiological indicators are combined into the physiological sensing vector expressed by Equation (2), which constitutes the physiological input to the proposed framework.

$$X_{phys}(t) = [CAP(t),\ IRR(t)] \tag{2}$$

$CAP(t)$ denotes the leaf capacitance response associated with transpiration dynamics and crop water status, whereas $IRR(t)$ represents the relative irradiance associated with incident solar radiation influencing plant physiological activity.

The physiological monitoring subsystem complements environmental observations by directly characterizing crop responses to changing environmental conditions. Consequently, physiological sensing provides additional information for crop stress assessment and serves as an essential input to the explainable decision-support model presented in Section 2.8. For experimental implementation, the proposed physiological monitoring subsystem was realized using the commercially available PI FylloClip® wearable leaf sensor integrating capacitance-based transpiration sensing and photodiode irradiance measurements.

2.4. AI-Based Pest-Monitoring Subsystem

The embedded AI pest-monitoring subsystem constitutes the third sensing layer of the proposed agricultural intelligence framework. Its primary objective is the autonomous acquisition of sticky-trap images and the generation of quantitative information on insect populations for continuous pest surveillance and subsequent integration into the decision-support framework. For the experimental implementation, pest monitoring was performed using the commercial iSCOUT system equipped with a 10 MP camera. High-resolution images of the sticky plate are acquired automatically under field conditions and transmitted via the mobile network to the FieldClimate platform (Pessl Instruments, Weiz, Austria), where proprietary AI-based insect detection and counting are performed. The resulting outputs provide information on detected insects and temporal pest-population dynamics. The underlying AI architecture, model version, training dataset, annotation protocol, and training/validation/test split are proprietary and are not publicly disclosed by the manufacturer. Accordingly, the present study did not develop, train, or independently validate the commercial pest-detection model; rather, its AI-generated detection and counting outputs were used as input data for the proposed decision-support framework.

According to the manufacturer's documentation, newly detected insects are identified relative to the previous image, while the FieldClimate platform provides summarized daily counts and temporal information on pest-population development. Therefore, the image-level detection count should not be interpreted as a continuously increasing cumulative count. In the present framework, the daily AI-generated monitoring outputs were used to derive the pest-density indicator, PD(t), which was subsequently integrated with the predicted PSI in the explainable decision-support layer. Figure 6 illustrates the printed circuit board (PCB) of the iSCOUT field unit used for image acquisition, device control, and wireless communication under field conditions.

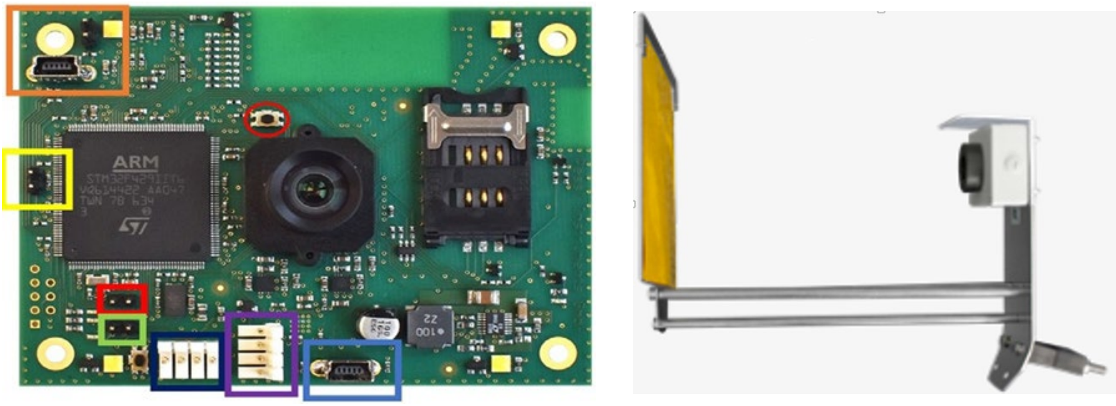

(**a**) (**b**)

Figure 6. Commercial iSCOUT pest-monitoring system: (**a**) physical printed circuit board (PCB); (**b**) field-deployable monitoring unit.

The principal hardware interfaces (Figure 6a) and their corresponding functions are summarized in Table 2.

Table 2. Principal hardware interfaces of the commercial iSCOUT AI-based pest-monitoring device.

Interface	Description
USB Service	Firmware maintenance
Boot Interface	Firmware installation
Modem Interface	Cellular communication
Terminal Interface	Device configuration
USB Port	Data communication
Expansion Connector	External peripherals
Control Connector	Embedded controller
Communication Button	Manual synchronization

The integrated hardware architecture enables autonomous image acquisition, wireless communication, and AI-assisted pest monitoring through the FieldClimate platform, supporting continuous pest surveillance under field conditions.

The pest-monitoring workflow consists of the following sequential stages: Image Acquisition → Image Transmission → Proprietary AI-Based Insect Detection and Counting → Pest-Density Estimation → Explainable Decision Support.

For each monitoring day d, the total pest count was calculated by aggregating the AI-generated insect counts reported by the commercial monitoring platform:

$$N_{pest}(t) = \sum_{i=1}^{n} D_i(t) \tag{3}$$

- $D_i(t)$ denotes the AI-generated count for the i-th reported insect group on monitoring day d.
- $N_{pest}(t)$ represents the total aggregated pest count for the corresponding monitoring day.

The daily pest counts were treated independently and were not accumulated across consecutive monitoring days. Therefore, $N_{pest}(d)$ represents pest activity for the corresponding day rather than a continuously increasing cumulative count. To normalize pest activity with respect to the monitored trap area, the pest density indicator is defined as

$$PD(t) = \frac{N_{pest}(t)}{A_{trap}} \tag{4}$$

where

- $N_{pest}(t)$ represents the aggregated AI-generated pest count for monitoring day d;

- A_{trap} denotes the effective monitoring area of the sticky trap.

Higher values of $PD(t)$ indicate increased pest activity and elevated crop-protection risk.

2.5. Communication and Cloud Infrastructure

The communication and cloud infrastructure provides wireless connectivity between the distributed field devices and the FieldClimate platform. The communication subsystem supports GSM, LTE, LTE-M, and Narrowband Internet of Things (NB-IoT), enabling autonomous transmission of environmental, physiological, and pest-monitoring data from the field devices.

The FieldClimate platform provides centralized data synchronization, storage, visualization and monitoring, and data access/export. Transmitted iSCOUT sticky-trap images are additionally processed using the proprietary AI pest-detection and counting software. The resulting pest-monitoring outputs are subsequently transferred to the analytical decision-support layer, where they are integrated with the environmental and physiological information. The complete processing workflow and separation between field sensing, cloud-based data management, and subsequent analytical decision-support processing are illustrated in Figure 7.

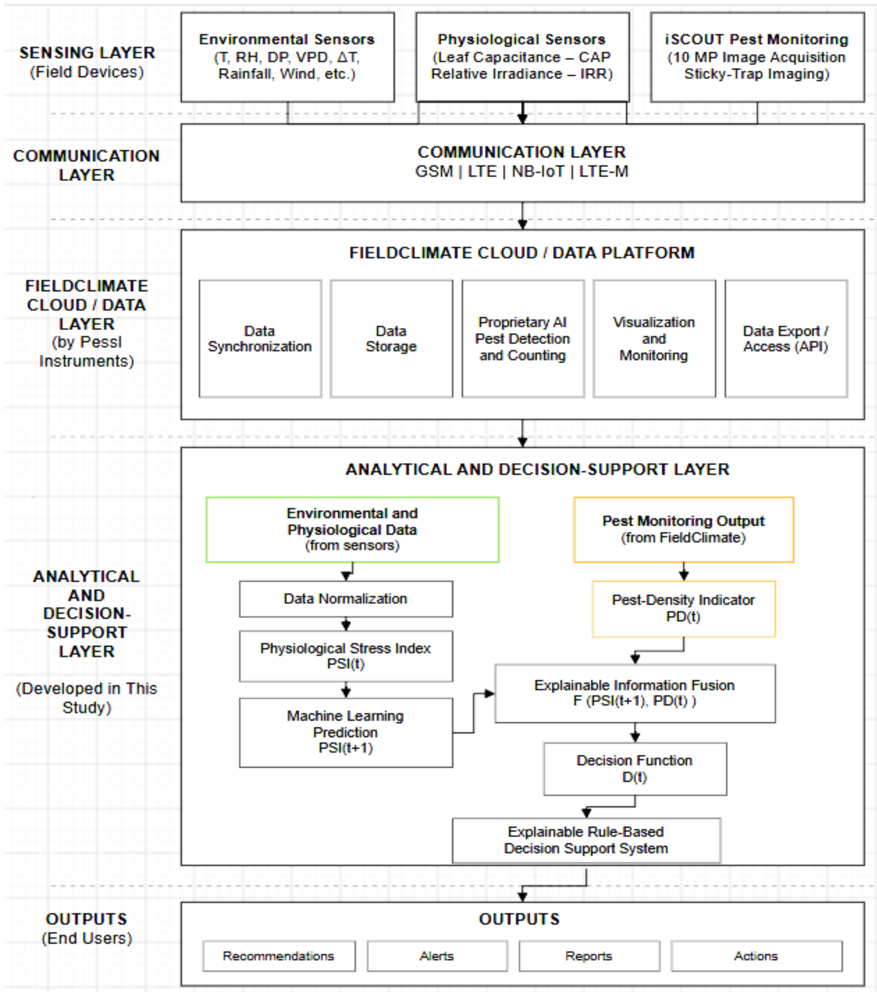

Figure 7. Layered processing architecture of the proposed agricultural intelligence framework, distinguishing field sensing, communication, FieldClimate cloud-based data management and proprietary pest detection, and subsequent analytical and explainable decision-support processing. Arrows indicate the direction of data and information flow, connecting lines represent communication and functional links, and colors distinguish the functional layers of the framework.

For experimental implementation, the proposed communication infrastructure was realized using a commercial nMETOS80 environmental monitoring station integrated with PI FylloClip® physiological sensors, CropView/iScout AI-based pest-monitoring devices, and the FieldClimate cloud platform. The principal hardware, communication, and deployment characteristics of the experimental platform are summarized in Table 3.

Table 3. Experimental deployment and communication characteristics of the proposed agricultural monitoring platform.

Characteristic	Value
Environmental monitoring station	nMETOS80
Physiological sensing	PI FylloClip® leaf sensor
AI pest monitoring	CropView/iScout
Firmware version	1.43
Hardware version	1.10
Communication modem	HL7802
Wireless communication	GSM (Preferred 2G/GSM)
Signal strength	68%
Logging interval	15 min
Data transfer interval	60 min
Monitoring mode	Continuous autonomous field monitoring
Data synchronization	Automatic cloud synchronization (FieldClimate platform)
Power supply	Solar panel + rechargeable battery
Battery operating voltage	3.1–3.6 V

2.6. Validation Methodology of the Proposed Physiological Stress Index

To assess the internal consistency of the proposed Physiological Stress Index (PSI), Pearson correlation analysis was performed between the calculated PSI values and their principal environmental and physiological components. Pearson's correlation coefficient was selected to quantify the strength and direction of the linear relationships between the proposed stress index and its constituent variables.

The Pearson correlation coefficient is defined as

$$r = \frac{\sum_{i=1}^{n}(x_i - \overline{x}_i)(y_i - \overline{y}_i)}{\sqrt{\sum_{i=1}^{n}(x_i - \overline{x}_i)^2}\sqrt{\sum_{i=1}^{n}(y_i - \overline{y}_i)^2}} \quad (5)$$

where

r is the Pearson correlation coefficient;
x_i and y_i denote paired observations;
$\overline{x}_i$ and $\overline{y}_i$ are the corresponding sample means;
n is the number of observations.

2.7. Machine-Learning Prediction of Physiological Stress

To extend the proposed framework from current physiological assessment toward anticipatory crop monitoring, machine-learning models were employed for short-term prediction of the PSI across multiple forecasting horizons. The environmental and physiological measurements were recorded at 15 min intervals and aligned by timestamp. Two FylloClip sensors were deployed on two separate pepper plants, with one sensor attached to a representative leaf of each plant. At each timestamp, the capacitance measurements from the two FylloClip sensors were averaged to obtain a representative CAP value, while the corresponding irradiance measurements were averaged to obtain a representative IRR value. Consequently, the two sensors did not generate separate observations in the machine-learning dataset; each timestamp constituted a single temporal observation containing the synchronized environmental variables and the averaged physiological indicators. During preprocessing, invalid or missing values in the variables required for modelling were excluded, the observations were chronologically ordered, and duplicate timestamps were removed. No separate statistical outlier-removal procedure was applied; valid field measurements were retained to preserve naturally occurring environmental and physiological variability. The resulting dataset contained 4893 valid synchronized temporal observations spanning 21 May 2026 at 08:00 to 11 July 2026 at 08:00. The one-step-ahead prediction problem was formulated as

$$\hat{PSI}\ (t+1) = f(VPD(t), RH(t), \Delta T(t), CAP(t), IRR(t), PSI(t)) \quad (6)$$

where $\hat{PSI}\ (t+1)$ denotes the predicted Physiological Stress Index, while $VPD(t)$, $RH(t)$, $\Delta T(t), CAP(t), IRR(t), PSI(t)$ represent the environmental, physiological, and stress-related information available at the current time step.

For one-step-ahead prediction, the feature vector at time t was temporally aligned with the PSI value at the immediately subsequent 15 min observation t + 1. The target sequence was therefore generated by shifting the PSI series by one time step. Because the final observation had no subsequent PSI value, it was excluded from model development, resulting in 4892 valid input-target pairs. The predictor vector included VPD, RH, Delta-T, averaged CAP, averaged IRR, and the current PSI at time t, whereas the target was PSI at time t + 1.

In addition to the one-step-ahead prediction, the same modelling framework was extended to multiple forecasting horizons of 30 min, 1 h, 1.5 h, and 2 h. Given the 15 min sampling interval, the corresponding target variables were generated by shifting the PSI sequence by 2, 4, 6, and 8 time steps, respectively, such that the prediction targets corresponded to PSI(t + 2), PSI(t + 4), PSI(t + 6), and PSI(t + 8). For each forecasting horizon, the predictor vector at time t remained unchanged and included VPD, RH, Delta-T, averaged CAP, averaged IRR, and the current PSI. Observations without an available future target at the respective horizon were excluded. The same chronological test forecast origin was retained across all forecasting horizons. Input–target pairs crossing the training–testing boundary were excluded, ensuring that all test targets occurred strictly after the common forecast origin and that the temporal separation between model development and evaluation was preserved.

Three regression algorithms were evaluated: Linear Regression, Random Forest Regression, and Gradient Boosting Regression. Linear Regression was selected as an interpretable reference model, whereas Random Forest and Gradient Boosting were employed to capture potentially nonlinear relationships between atmospheric conditions, plant physiological responses, and future stress dynamics. A persistence baseline was also included, assuming that the future physiological stress remains equal to the current PSI value:

$$\hat{PSI}\ (t+1) = PSI(t) \quad (7)$$

For the one-step-ahead analysis, the 4892 input–target pairs were divided chronologically rather than randomly. The first 3424 pairs (70%) were used for model training, while the remaining 1468 pairs (30%) were reserved for independent testing. The training input observations extended through 26 June 2026 at 00:45, and the test forecast origin was defined at 26 June 2026 at 01:00. The corresponding one-step-ahead target sequence extended through the final PSI observation recorded on 11 July 2026 at 08:00. To prevent preprocessing-related information leakage, the chronological training–testing boundary was defined before PSI normalization. The minimum and maximum values required for

PSI calculation were estimated exclusively from the 3424 training input observations and subsequently applied unchanged to the test observations. Test-set extrema were not used to determine any normalization parameter. Test observations outside the training-derived ranges were clipped to the interval [0, 1] to preserve the predefined PSI scale. This procedure ensured that neither model fitting nor PSI normalization incorporated information from the future test period.

Model performance was evaluated using the mean absolute error (MAE), root mean squared error (RMSE), and coefficient of determination (R^2):

$$MAE = \frac{1}{n}\sum_{i=1}^{n}\left|PSI_i - P\hat{S}I_i\right| \tag{8}$$

$$RMSE = \sqrt{\frac{1}{n}\sum_{i=1}^{n}\left(PSI_i - P\hat{S}I_i\right)^2} \tag{9}$$

$$R^2 = 1 - \frac{\sum_{i=1}^{n}\left(PSI_i - P\hat{S}I_i\right)^2}{\sum_{i=1}^{n}\left(PSI_i - \overline{PSI_i}\right)^2} \tag{10}$$

where PSI_i and $P\hat{S}I_i$ denote the observed and predicted PSI values, respectively, $\overline{PSI_i}$ represents the mean of the observed PSI values, and n is the number of observations.

In addition to the chronological holdout evaluation, three-fold time-series cross-validation was performed to further assess model robustness and generalization across different temporal partitions. Three folds were selected to preserve the chronological structure of the dataset while maintaining sufficiently large training and testing partitions for reliable model evaluation. Within the three-fold time-series cross-validation procedure, PSI normalization was repeated independently for each fold. The minimum and maximum values were calculated exclusively from the corresponding fold's training input observations and subsequently applied unchanged to that fold's validation observations.

All computational analyses were performed in Python 3.10.19 within an Anaconda environment (conda 25.11.1) and Jupyter Notebook 7.4.5, environment using NumPy 1.26.4, pandas 2.1.4, scikit-learn 1.7.2, and Matplotlib 3.7.5. The machine-learning implementation used the LinearRegression, RandomForestRegressor, GradientBoostingRegressor, and TimeSeriesSplit classes provided by scikit-learn.

2.8. Decision-Support Model

The final layer of the proposed hybrid intelligent framework integrates machine-learning prediction of the Physiological Stress Index (PSI) with an explainable rule-based decision-support model. It combines multimodal sensing information obtained from the environmental monitoring, plant physiological monitoring, and embedded AI-based pest-monitoring subsystems to generate transparent and interpretable agronomic recommendations for precision agriculture applications.

The multimodal agricultural sensing vector is defined as

$$X_{agri}(t) = \left[X_{env}(t), X_{phys}(t)\right] \tag{11}$$

or equivalently:

$$X_{agri}(t) = [P(t), T(t), RH(t), SM(t), LW(t), DP(t), VPD(t), \Delta T(t), CAP(t), IRR(t)] \tag{12}$$

where

$X_{env}(t)$ denotes the environmental sensing vector;

$X_{phys}(t)$ denotes the physiological sensing vector.

To quantify crop physiological conditions, the environmental and physiological measurements are combined into a Physiological Stress Index (PSI). Prior to index calculation, all sensing variables are normalized according to

$$x_n(t) = \frac{x(t) - x_{min}}{x_{max} - x_{min}} \tag{13}$$

where

- $x_n(t)$ denotes the normalized variable value;
- $x(t)$ denotes the measured variable;
- x_{min} represents the minimum observed value;
- x_{max} represents the maximum observed value.

For the predictive analysis, the chronological training–testing boundary was defined before normalization. The values of x_{min} and x_{max} for each PSI component were calculated exclusively from the training input observations. These training-derived parameters were subsequently applied unchanged to both the training and testing observations. Test observations outside the training range were clipped to the interval [0, 1] without recalculating any normalization parameter from the test data. The resulting PSI series was then used to generate the forecasting targets. In the time-series cross-validation analysis, the normalization procedure was repeated independently within each fold using only the corresponding fold's training observations.

The proposed Physiological Stress Index is expressed as

$$PSI(t) = 0.30\, VPD_n(t) + 0.25\, RH_{stress,n}(t) + 0.10\, CAP_n(t) + 0.15\, IRR_n(t) + 0.20\, \Delta T_n(t) \tag{14}$$

where the relative-humidity stress component is defined as

$$RH_{stress,n}(t) = 1 - RH_n(t) \tag{15}$$

where

- $VPD_n(t)$ denotes normalized vapor pressure deficit;
- $RH_n(t)$ denotes normalized relative humidity;
- $RH_{stress,n}(t)$ inverse relative-humidity stress component;
- $CAP_n(t)$ denotes normalized leaf capacitance response;
- $IRR_n(t)$ denotes normalized relative irradiance;
- $\Delta T_n(t)$ denotes normalized Delta-T.

The PSI formulation follows the established physiological rationale of crop water-stress assessment, in which atmospheric evaporative demand and temperature-related variables play a major role in characterizing crop stress. In particular, VPD and temperature differences have been widely used as key components of crop water-stress assessment, including the development of the Crop Water Stress Index (CWSI) [39,40]. Accordingly, greater relative importance was assigned to VPD, inverse RH, and Delta-T, while IRR and CAP were incorporated as complementary sensing components reflecting radiation exposure and plant physiological response. Recent developments in wearable plant sensing further support the integration of direct plant-response measurements with environmental information for continuous crop water-status and stress monitoring [41,42].

The specific weighting coefficients (0.30, 0.25, 0.10, 0.15, and 0.20 for VPD, inverse RH, CAP, IRR, and Delta-T, respectively) were specified a priori as an initial heuristic proof-of-concept configuration rather than statistically estimated or optimized from the experimental dataset. All weights are non-negative and sum to unity. Relative humidity is incorporated inversely because increasing RH corresponds to lower atmospheric evaporative demand

and consequently a lower contribution to physiological stress. The machine-learning models were not used to determine or optimize these weights; they were subsequently employed to predict the calculated PSI.

To support explainable agricultural decision making, the predicted physiological stress is integrated with the pest-density indicator through the explainable information-fusion function:

$$D(t) = F(\hat{PSI}(t+1),\ PD(t)) \tag{16}$$

$F(\cdot)$ denotes the explainable information-fusion function.

The explainable fusion function evaluates the predicted physiological stress level together with the normalized pest-density level according to the predefined transparent rule base, producing the final agronomic recommendation.

The proposed explainable decision-support model combines the predicted Physiological Stress Index with the normalized pest-density indicator into a unified decision layer that generates transparent and interpretable agronomic recommendations for precision agriculture applications.

3. Results

3.1. Environmental Monitoring Results

The environmental monitoring subsystem continuously acquired the principal atmospheric and microclimatic variables required for precision agriculture, including air temperature, relative humidity, dew point, vapor pressure deficit (VPD), and Delta-T. These parameters were continuously monitored during field deployment and subsequently analyzed to evaluate the environmental conditions affecting crop physiological responses and agricultural decision support. Representative monitoring results are presented in Figure 8.

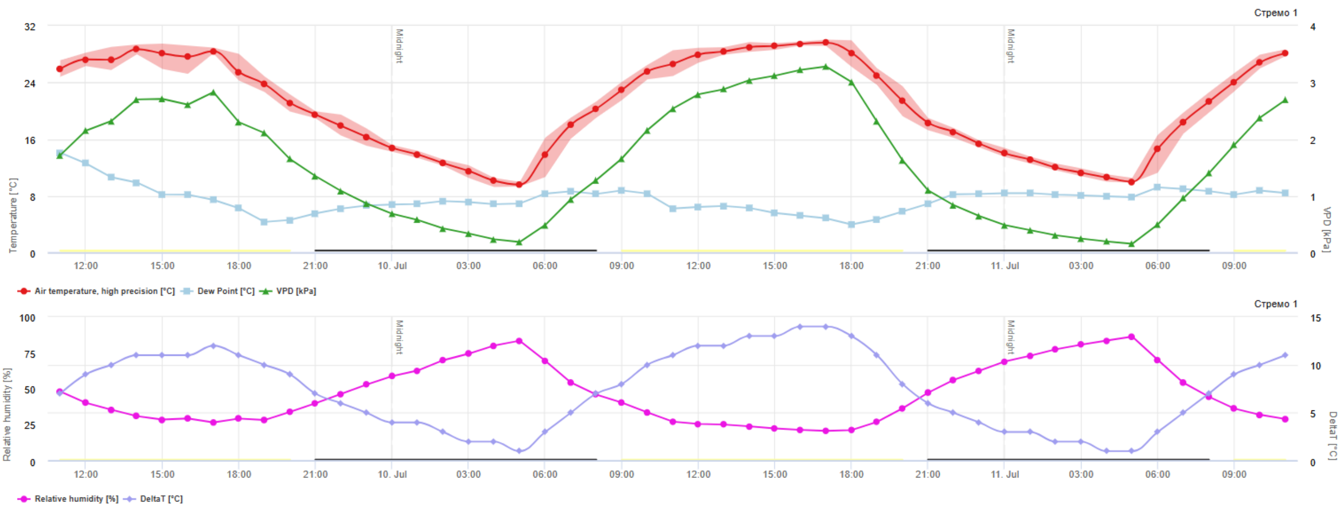

Figure 8. Representative environmental monitoring results showing air temperature (red; °C), dew point (light blue; °C), vapor pressure deficit (green; kPa), relative humidity (magenta; %), and Delta-T (light violet; °C), acquired during a 48 h field-monitoring period. The yellow and black horizontal bars along the time axis indicate daytime and nighttime periods, respectively. The label "Стремо 1" is the automatically generated Cyrillic station name displayed by the FieldClimate platform and corresponds to "STREMO Station 1" in English.

The monitored variables exhibit the expected diurnal behavior, characterized by increasing daytime air temperatures accompanied by decreasing relative humidity and increasing vapor pressure deficit (VPD). The observed environmental dynamics demonstrate the capability of the proposed monitoring subsystem to continuously capture atmospheric conditions relevant for physiological stress assessment and agricultural decision support.

A clear inverse relationship between air temperature and relative humidity was observed throughout the monitoring period. The highest VPD values occurred during the warmest daytime hours, indicating increased atmospheric evaporative demand, whereas nighttime conditions were characterized by lower temperatures, higher relative humidity, and substantially reduced VPD values. These environmental measurements constitute the primary inputs to the proposed Physiological Stress Index (PSI) and provide the environmental context for the integrated physiological monitoring and explainable decision-support framework presented in the following sections.

3.2. Plant Physiological Monitoring Results

In addition to environmental monitoring, the proposed framework continuously acquired plant physiological responses using wearable leaf sensors. Two physiological indicators, namely leaf capacitance (CAP) and relative irradiance (IRR), were continuously monitored throughout the observation period to characterize plant transpiration dynamics and crop responses to changing environmental conditions. Representative physiological monitoring results are presented in Figure 9.

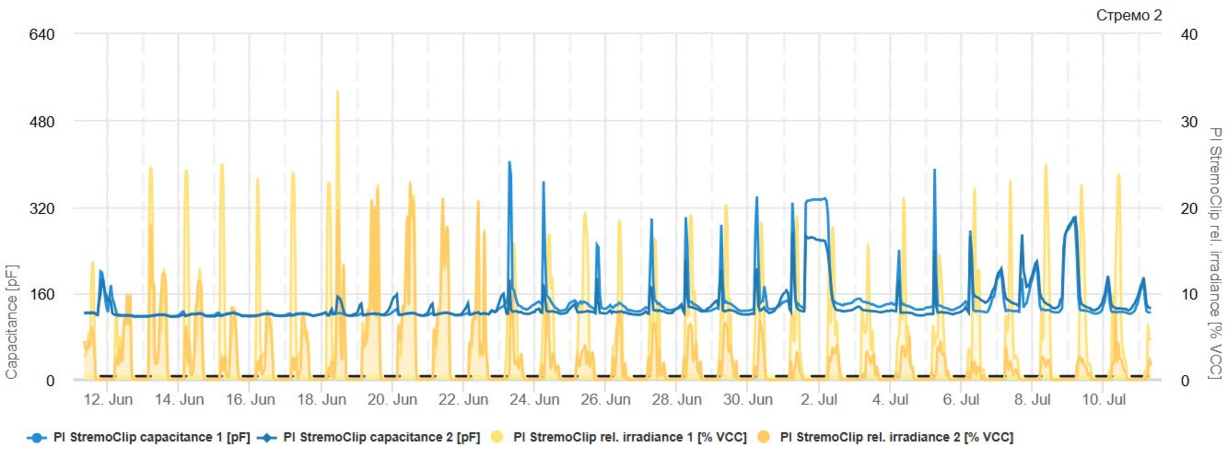

Figure 9. Long-term physiological monitoring results showing leaf capacitance (CAP) from sensor 1 (blue line with circular markers) and sensor 2 (dark-blue line with diamond markers), and relative irradiance (IRR) from sensor 1 (yellow line with circular markers) and sensor 2 (orange line with circular markers), measured over a 30-day field deployment.

The figure presents the capability of the proposed physiological monitoring subsystem to continuously assess plant responses under long-term field conditions. The continuous recordings demonstrate the capability of the wearable sensing platform throughout the 30-day deployment.

The monitored leaf capacitance (CAP) and relative irradiance (IRR) exhibited clear temporal variations throughout the observation period, reflecting changes in plant physiological activity under naturally varying environmental conditions. These physiological measurements complement the environmental monitoring data and enable continuous assessment of plant transpiration behavior and crop responses.

Periods of increased atmospheric evaporative demand corresponded to noticeable variations in both leaf capacitance and relative irradiance, demonstrating the sensitivity of the physiological sensing subsystem to changing environmental conditions. These findings confirm the effectiveness of the proposed multimodal sensing framework for continuous crop monitoring and provide complementary physiological information that is subsequently integrated into the Physiological Stress Index (PSI) and the explainable decision-support framework.

3.3. Correlation Analysis Between Environmental and Physiological Variables

To further investigate the relationship between environmental conditions and plant physiological responses, a Pearson correlation analysis was performed using the monitored environmental variables together with the corresponding physiological indicators measured by the wearable leaf sensors. The analysis included air temperature, relative humidity, vapor pressure deficit (VPD), and Delta-T together with leaf capacitance (CAP) and relative irradiance (IRR) obtained from two independently monitored pepper leaves.

Figure 10 provides an overview of the relationships between the monitored environmental variables and the physiological indicators derived from the wearable sensing subsystem.

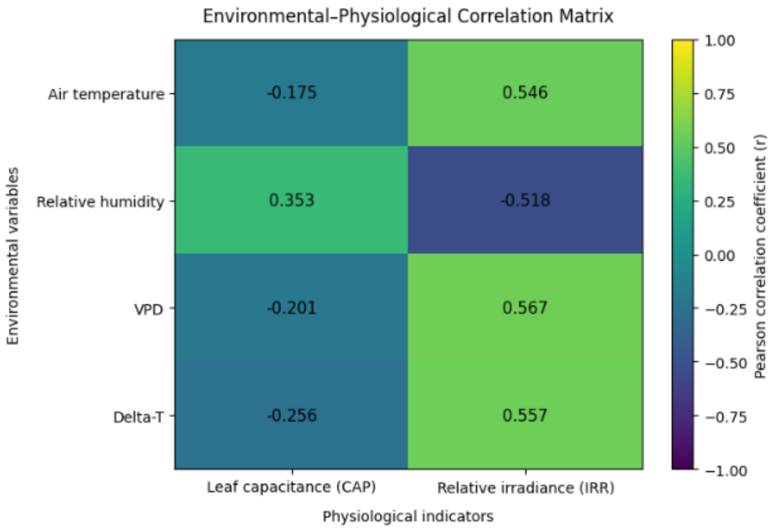

Figure 10. Pearson correlation matrix between the monitored environmental variables and physiological indicators measured on pepper leaves during field deployment.

As illustrated in Figure 10, IRR exhibited stronger correlations with the monitored environmental variables than CAP, indicating that the optical physiological measurements were more responsive to short-term environmental fluctuations.

The correlation analysis confirmed the expected relationships among the monitored environmental variables. Air temperature exhibited a strong positive correlation with vapor pressure deficit ($r = 0.942$) and Delta-T ($r = 0.912$), whereas relative humidity showed strong negative correlations with VPD ($r = -0.924$) and Delta-T ($r = -0.967$). These findings are consistent with the well-established physical relationships governing agricultural microclimates and confirm the reliability of the environmental monitoring subsystem.

The physiological indicators exhibited different sensitivities to the monitored environmental conditions (Table 4). As summarized in Table 4, relative irradiance (IRR) demonstrated moderate positive correlations with air temperature ($r = 0.546$), vapor pressure deficit ($r = 0.567$), and Delta-T ($r = 0.557$), together with a moderate negative correlation with relative humidity ($r = -0.518$). These results indicate that the optical physiological measurements closely followed the environmental dynamics during the monitoring period.

In contrast, leaf capacitance (CAP) exhibited weaker correlations with the monitored environmental variables, with correlation coefficients ranging from -0.256 to 0.353. This behavior suggests that capacitance-based measurements reflect more complex physiological processes that cannot be explained solely by atmospheric conditions. Unlike irradiance measurements, leaf capacitance is additionally influenced by internal plant water status, transpiration dynamics, and other physiological mechanisms, resulting in lower direct correlations with individual environmental variables.

Table 4. Pearson correlation coefficients between environmental variables and physiological indicators.

Environmental Variable	CAP (*r*)	*p*-Value	IRR (*r*)	*p*-Value
Air Temperature	−0.175	<0.001	0.546	<0.001
Relative Humidity	0.353	<0.001	−0.518	<0.001
VPD	−0.201	<0.001	0.567	<0.001
Delta-T	−0.256	<0.001	0.557	<0.001

Overall, the obtained correlation patterns demonstrate that environmental monitoring and physiological sensing provide complementary information regarding crop status. Environmental variables characterize the external atmospheric conditions, whereas physiological indicators directly reflect crop responses to these conditions. Consequently, the integration of both sensing modalities establishes a scientifically justified basis for the proposed multimodal agricultural intelligence framework and provides the physiological information required by the explainable decision-support model developed in this study.

3.4. Embedded AI Pest-Monitoring Results

The embedded AI pest-monitoring subsystem continuously performed autonomous image acquisition and insect detection under field conditions. Captured images were processed using the proprietary AI-based detection and counting functionality of the commercial monitoring platform to identify insect objects, estimate pest density, and generate quantitative information for pest assessment. Figure 11 presents representative AI-based insect detection results obtained during the experimental monitoring period. Figure 11a shows the field image together with the total number of detected insects, whereas Figure 11b presents the detailed AI detection output including insect localization and classification generated by the embedded AI system.

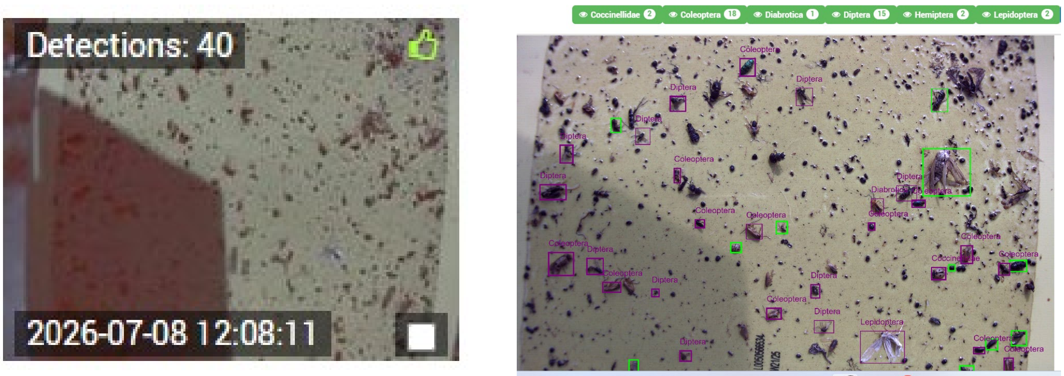

(**a**) (**b**)

Figure 11. Representative AI-based insect detection results obtained from sticky-trap images acquired by the commercial CropView/iSCOUT embedded pest-monitoring subsystem under field conditions: (**a**) field image showing the total number of detected insects; (**b**) detailed AI detection output showing insect localization and classification.

The embedded monitoring device successfully acquired field images throughout the observation period without manual intervention. Continuous image acquisition enabled automated surveillance of crop surroundings and provided the input required for subsequent AI-based pest detection and quantitative population analysis.

Figure 12 illustrates the temporal evolution of representative insect populations detected by the embedded AI monitoring subsystem. Coleoptera and Diptera exhibited the highest population densities throughout the observation period, whereas the remaining insect groups were observed at substantially lower frequencies.

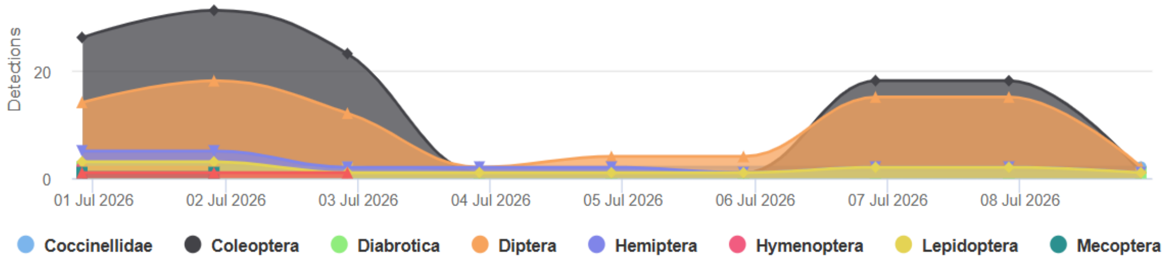

Figure 12. Temporal dynamics of representative insect populations automatically detected by the embedded AI pest-monitoring subsystem during the field observation period. The colored circles in the legend identify the insect groups by color. The point symbols displayed along the curves are automatically generated by the monitoring platform and do not represent additional categories.

The detected temporal variations illustrate the pest-monitoring outputs generated by the commercial embedded AI platform during autonomous field deployment and provide the pest-density information subsequently used by the proposed decision-support framework. The normalized pest-density indicator PD(t) was subsequently integrated with the Physiological Stress Index (PSI) to support explainable agricultural decision making.

3.5. Physiological Stress Assessment Using the Physiological Stress Index (PSI)

The proposed physiological stress assessment framework was applied to real-time measurements acquired from the STREMO environmental monitoring station equipped with dual FylloClip leaf sensors. The Physiological Stress Index (PSI) integrates atmospheric demand variables, including vapor pressure deficit (VPD), relative humidity (RH), and Delta-T, with direct plant-response indicators derived from leaf capacitance (CAP) and relative irradiance (IRR). The resulting dimensionless index ranges from 0 to 1 and was classified into low, medium, and high stress levels to support transparent interpretation. Based on the normalized environmental and physiological variables defined in the methodological framework, PSI values were calculated for the complete field monitoring dataset collected between 21 May and 11 July 2026 in Figure 13.

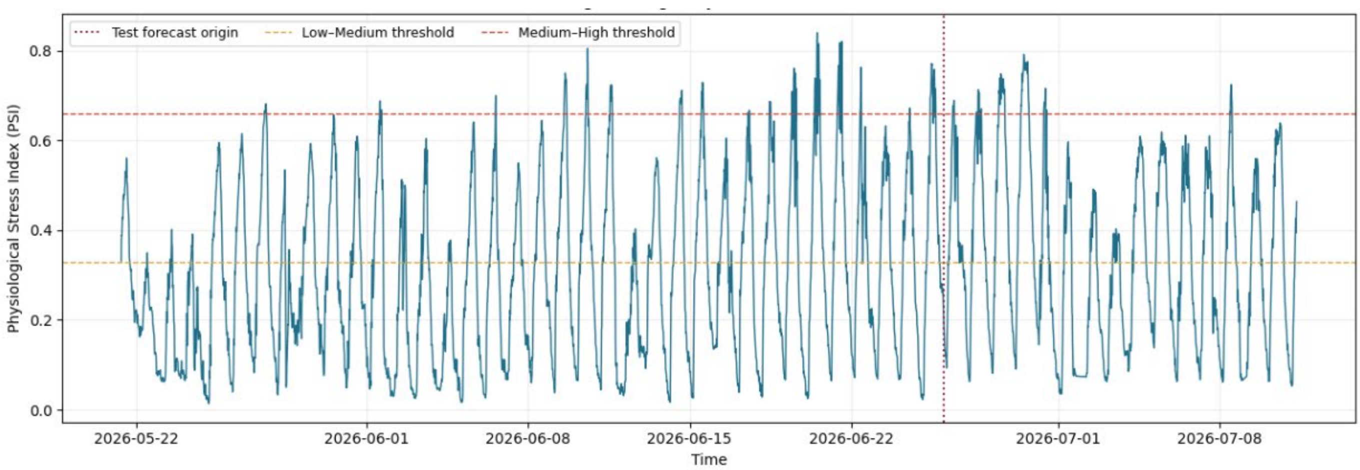

Figure 13. Temporal variation in the Physiological Stress Index (PSI) during the field monitoring campaign conducted between 21 May and 11 July 2026. Dashed horizontal lines indicate the thresholds separating low, medium, and high physiological stress levels.

The temporal profile of the Physiological Stress Index (PSI) exhibited a clear diurnal pattern throughout the monitoring campaign. In general, PSI values increased during daytime periods, when higher air temperature and vapor pressure deficit (VPD) were accompanied by lower relative humidity, and decreased during the evening and nighttime hours as atmospheric demand was reduced. Transient episodes of elevated physiological stress (PSI $\geq$ 0.66) were observed during periods of increased evaporative demand, demonstrating that the proposed index consistently responded to changing environmental conditions.

The descriptive statistics of the calculated PSI values are summarized in Table 5. A total of 4893 synchronized environmental and physiological observations were analyzed. Following training-only normalization, PSI values ranged from 0.014 to 0.840, with a mean of 0.310 and a standard deviation of 0.195. The median PSI was 0.282, while the interquartile range extended from 0.137 to 0.465.

Table 5. Descriptive statistics of the PSI.

Statistic	Value
Number of observations	4893
Mean PSI	0.310
Standard deviation	0.195
Minimum PSI	0.014
25th percentile	0.137
Median	0.282
75th percentile	0.465
Maximum PSI	0.840

To facilitate interpretation within the proposed explainable decision-support framework, PSI values were classified into low, medium, and high physiological stress categories, as summarized in Table 6. The distribution of the three stress levels provides an overview of the frequency of different physiological conditions observed during the complete monitoring period and forms the basis for the subsequent integration with AI-based pest monitoring in the explainable DSS.

Table 6. Distribution of PSI.

PSI Category	Number of Observations	Percentage (%)
Low	2821	57.7
Medium	1834	37.5
High	238	4.9
Total	4893	100.0

Figure 13 together with Tables 5 and 6 demonstrates that the proposed PSI captures both continuous temporal variation and categorical stress severity. The PSI therefore provides the physiological input to the explainable DSS, complementing the normalized pest-density indicator derived from the embedded AI monitoring subsystem. Their joint interpretation is presented in the following subsection.

3.6. Validation and Sensitivity Analysis of the Proposed Physiological Stress Index

To further evaluate the proposed Physiological Stress Index, an internal validation and sensitivity analysis was performed using Pearson correlation between PSI and its principal environmental and physiological components. The objective of this analysis was to verify whether the proposed index responds consistently to variations in atmospheric demand and plant physiological activity. The obtained correlation coefficients are summarized in Table 7.

Table 7. Pearson correlation between PSI and the environmental and physiological variables.

Variable	Pearson (r)	p-Value	Interpretation
Vapor Pressure Deficit (VPD)	0.980	<0.001	Strong positive
Relative Humidity (RH)	−0.961	<0.001	Strong negative
Delta-T	0.990	<0.001	Strong positive
Leaf Capacitance (CAP)	−0.215	<0.001	Weak negative
Relative Irradiance (IRR)	0.553	<0.001	Moderate positive

The revised PSI exhibited strong positive correlations with vapor pressure deficit (r = 0.980) and Delta-T (r = 0.990), together with a strong negative correlation with relative humidity (r = −0.961). A weak negative correlation was observed with leaf capacitance (r = −0.215), whereas relative irradiance showed a moderate positive correlation (r = 0.553).

These relationships are generally consistent with the physiological processes governing crop transpiration and water stress. Increasing atmospheric evaporative demand, reflected by higher VPD and Delta-T values together with decreasing relative humidity, resulted in increased PSI values, whereas the physiological indicators CAP and IRR provided complementary information regarding the internal physiological condition of the monitored crop. The weak negative empirical correlation between CAP and PSI does not imply a negative coefficient in the PSI formulation; rather, it reflects the marginal relationship between the measured capacitance signal and the multivariable composite PSI under the observed field conditions.

Since the proposed PSI is mathematically derived from these environmental and physiological variables, the observed correlations should be interpreted as evidence of the internal consistency and sensitivity of the proposed index rather than as an independent external validation. Nevertheless, the obtained results demonstrate that the proposed formulation responds consistently to changes in both atmospheric demand and plant physiological activity, supporting its suitability for subsequent machine-learning prediction and explainable decision support.

3.7. The Results of Machine-Learning Prediction of Physiological Stress

The machine-learning prediction framework described in Section 2.7 was evaluated using three regression algorithms to assess their capability for one-step-ahead prediction of the proposed Physiological Stress Index. The comparative performance of the evaluated models is summarized in Table 8.

Table 8. Model performance comparison of machine-learning models for one-step-ahead PSI prediction.

Model	MAE	RMSE	(R^2)
Gradient Boosting	0.0189	0.0273	0.9810
Linear Regression	0.0186	0.0274	0.9808
Persistence baseline	0.0183	0.0276	0.9805
Random Forest Regression	0.0207	0.0297	0.9775

At the 15 min forecasting horizon, Linear Regression and Gradient Boosting demonstrated virtually identical predictive performance. Gradient Boosting achieved marginally better RMSE and R^2 values, whereas the persistence baseline produced the lowest MAE. The competitive performance of the persistence baseline confirms the strong short-term temporal continuity of the PSI signal.

Figure 14 illustrates the temporal behavior of Linear Regression and Gradient Boosting at the two selected forecasting horizons. Both models closely followed the observed PSI dynamics at the 15 min horizon. At the 1 h horizon, prediction errors became more pronounced, particularly for Linear Regression, whereas Gradient Boosting retained closer agreement with the observed temporal patterns across both the representative and complete test periods.

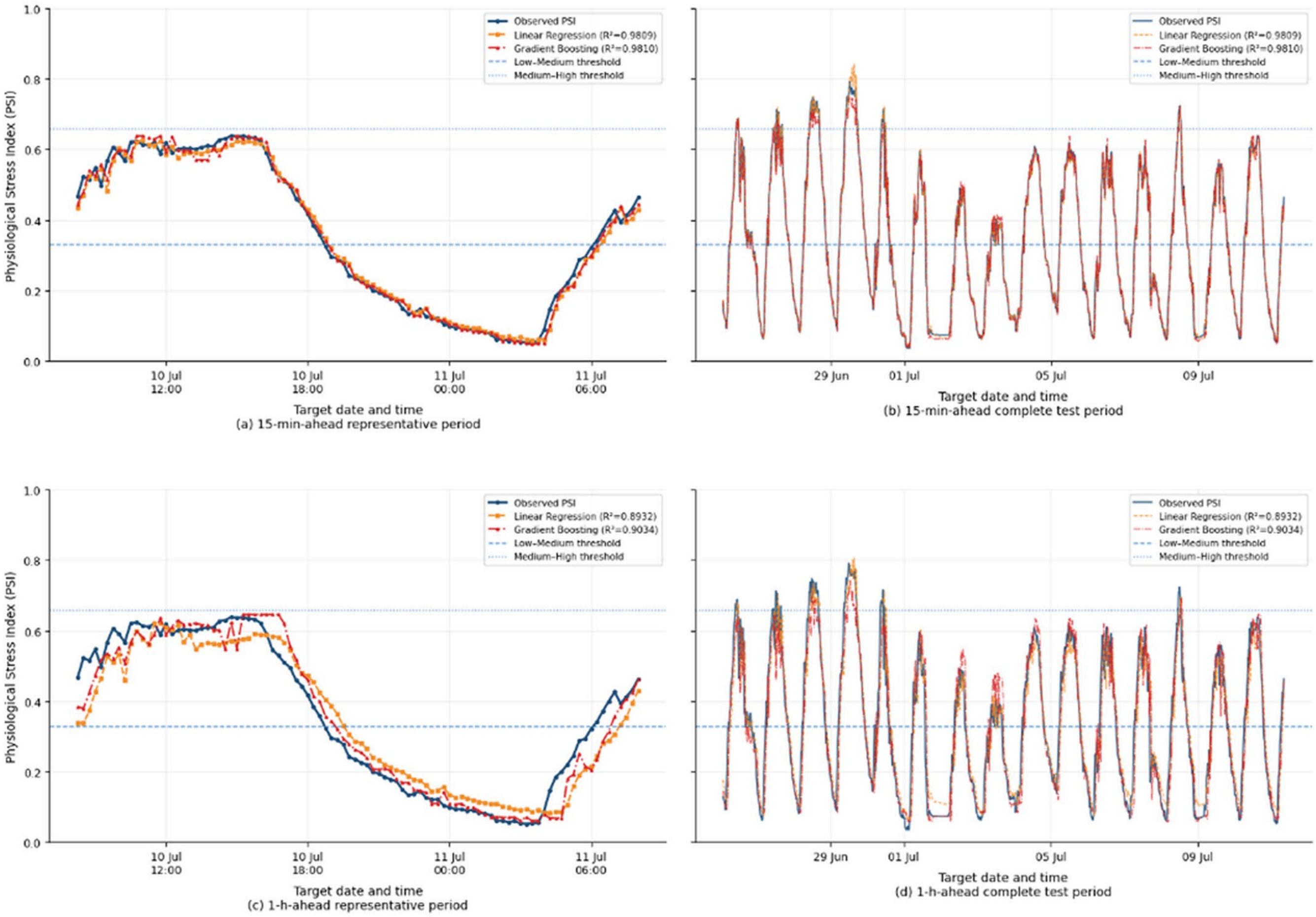

Figure 14. Temporal comparison of observed and predicted Physiological Stress Index (PSI) using Linear Regression and Gradient Boosting at the 15 min and 1 h forecasting horizons. Representative and complete chronological test periods are shown.

The agreement between observed and predicted PSI values is further examined in Figure 15. At the 15 min horizon, the predictions of both models were closely distributed around the identity line, confirming their virtually identical short-term performance. At the 1 h horizon, the dispersion increased, particularly at higher PSI values; however, Gradient Boosting maintained closer agreement with the observed values than Linear Regression. The scatter plots therefore corroborate the holdout metrics and demonstrate the expected horizon-dependent reduction in predictive accuracy.

To further evaluate model robustness beyond the holdout-test results, an additional three-fold time-series cross-validation was performed using chronological data partitions. The corresponding performance metrics are summarized in Table 9.

Table 9. Time-series cross-validation performance of the evaluated regression models.

Model	Mean MAE	SD	Mean RMSE	SD	Mean (R^2)	SD
Gradient Boosting Regression	0.0208	0.0027	0.0307	0.0054	0.9785	0.0070
Linear Regression	0.0205	0.0032	0.0309	0.0064	0.9781	0.0086
Random Forest Regression	0.0216	0.0027	0.0319	0.0048	0.9768	0.0067

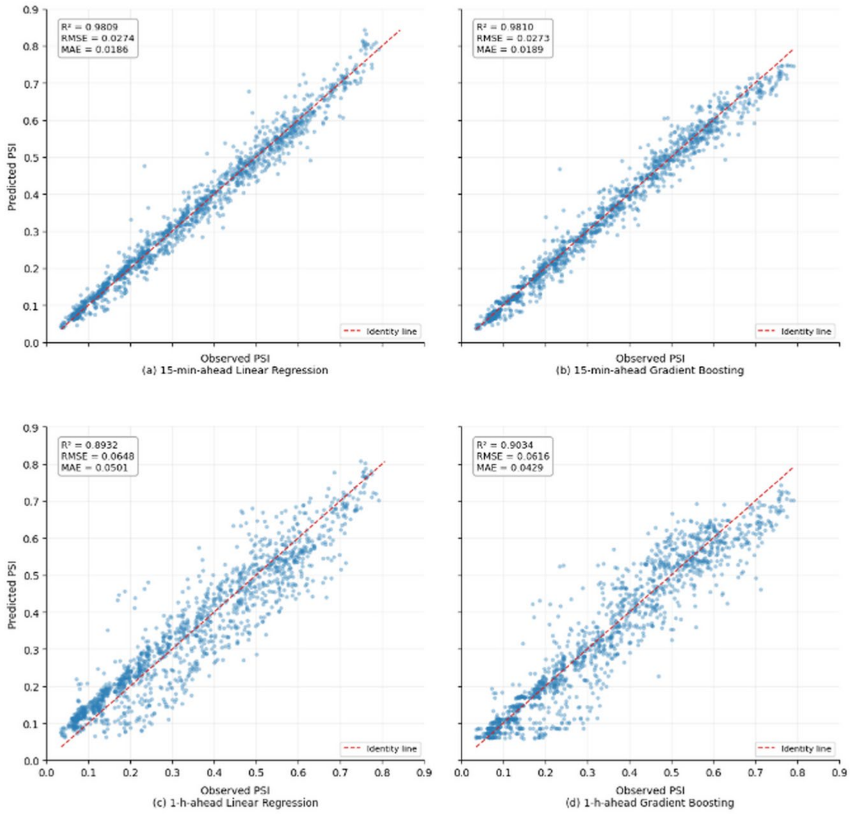

Figure 15. Observed versus predicted Physiological Stress Index (PSI) using Linear Regression and Gradient Boosting at the 15 min and 1 h forecasting horizons. The dashed diagonal line represents perfect agreement between observed and predicted values. The blue points represent individual observed–predicted PSI pairs, while the red dashed identity line indicates perfect agreement between the observed and predicted values.

The leakage-safe three-fold time-series cross-validation demonstrated consistently high predictive performance. Gradient Boosting achieved the lowest mean RMSE (0.0307) and the highest mean R^2 (0.9785), whereas Linear Regression achieved a marginally lower mean MAE (0.0205). The small differences between the models indicate stable one-step-ahead predictive performance across the chronological folds.

The relatively small standard deviations of MAE, RMSE, and R^2 indicate stable model performance across the chronological folds, demonstrating that the predictive relationships were consistently preserved throughout different temporal segments of the monitoring campaign. The slightly better average performance of Linear Regression suggests that one-step-ahead PSI prediction exhibits a strong short-term linear structure, which is expected because PSI at time $t + 1$ is closely related to the current PSI value and to environmental and physiological variables that change gradually between consecutive 15 min observations. However, the comparable performance of Gradient Boosting suggests that nonlinear relationships may become increasingly relevant at longer forecasting horizons.

The multi-horizon analysis confirmed that model performance depended on the forecasting horizon. Linear Regression achieved the strongest performance at the 30 min horizon (R^2 = 0.9541), whereas Gradient Boosting achieved the strongest performance from the 1 h horizon onward. Gradient Boosting achieved R^2 values of 0.9034, 0.8366, and 0.7531 at the 1 h, 1.5 h, and 2 h horizons, respectively, compared with persistence-baseline R^2 values of 0.8800, 0.7867, and 0.6666.

Overall, the cross-validation and multi-horizon results demonstrate robust short-term predictive performance while also showing that model behavior depends on the forecasting horizon. Linear Regression showed the strongest overall performance at the shorter 15 and 30 min horizons, whereas Gradient Boosting provided the strongest overall performance from the 1 h horizon onward.

Predictor contributions were examined for Linear Regression and Gradient Boosting at the 1 h forecasting horizon to investigate differences in their predictive structures. Absolute standardized coefficients were used to quantify the relative contributions within the Linear Regression model, whereas native feature-importance scores were used for Gradient Boosting (Figure 16).

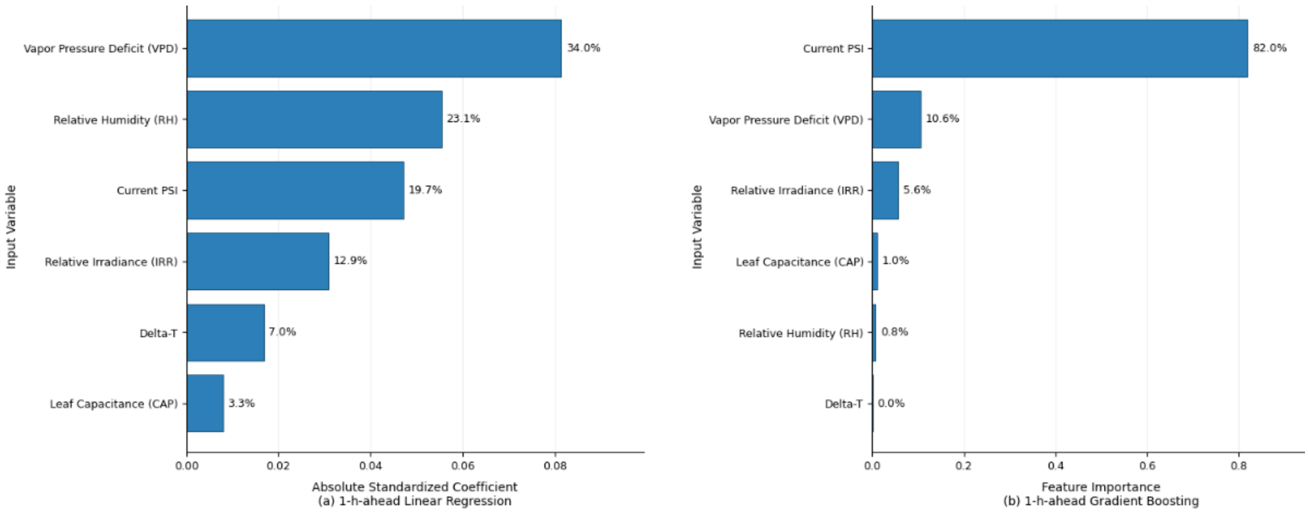

Figure 16. Model-specific predictor contributions for 1 h-ahead PSI prediction: (**a**) relative contributions based on the absolute standardized Linear Regression coefficients; (**b**) native Gradient Boosting feature importance.

For the 1 h Linear Regression model, VPD showed the largest relative contribution (34.0%), followed by relative humidity (23.1%), current PSI (19.7%), relative irradiance (12.9%), Delta-T (7.0%), and leaf capacitance (3.3%). In contrast, the 1 h Gradient Boosting model was predominantly influenced by current PSI (82.0%), followed by VPD (10.6%) and relative irradiance (5.6%). Leaf capacitance (1.0%), relative humidity (0.8%), and Delta-T (<0.1%) showed substantially smaller feature-importance values. These findings indicate that Linear Regression distributed its predictive dependence more broadly across the atmospheric and physiological variables, whereas Gradient Boosting primarily exploited the nonlinear predictive information contained in the current PSI, supplemented by VPD and irradiance.

The contribution percentages obtained for the two models are not directly comparable because they were derived using different model-specific interpretation measures. For Linear Regression, the reported percentages were calculated from the absolute standardized regression coefficients, whereas the Gradient Boosting percentages represent native tree-based feature-importance scores. The results should therefore be interpreted within each model rather than as direct numerical comparisons between the models.

3.8. Explainable Decision-Support Demonstration (DSS)

The proposed DSS integrates the two complementary information sources developed in the previous subsections. The embedded AI pest-monitoring subsystem provides a normalized pest-density indicator, PD(t), derived from continuous insect detection and population quantification, whereas the physiological monitoring subsystem generates the

PSI, representing the current physiological condition of the monitored crop. Together, these complementary indicators provide a comprehensive description of both external biotic pressure and internal plant response. Unlike conventional black-box decision-support systems, the proposed framework employs transparent and interpretable decision rules. Each recommendation is generated from explicitly defined relationships between the physiological stress level and the observed pest density, allowing every system decision to be directly explained and verified by agronomists and end users. This approach improves interpretability, facilitates expert validation, and increases user confidence in autonomous agricultural decision making.

The explainable decision logic operates on two normalized indicators, PSI and PD, each represented by three overlapping fuzzy linguistic levels (low, medium, and high). Trapezoidal membership functions were defined over the normalized interval [0, 1] to provide gradual transitions between adjacent physiological-stress and pest-density levels, thereby avoiding abrupt changes associated with purely crisp thresholds. For each PSI–PD combination, the activation strength of the corresponding rule was calculated using the minimum operator. Because the rule consequents are linguistic agronomic recommendations rather than continuous numerical outputs, the recommendation associated with the highest activated rule was selected as the final decision-support output. The membership functions adopted for both normalized inputs are illustrated in Figure 17.

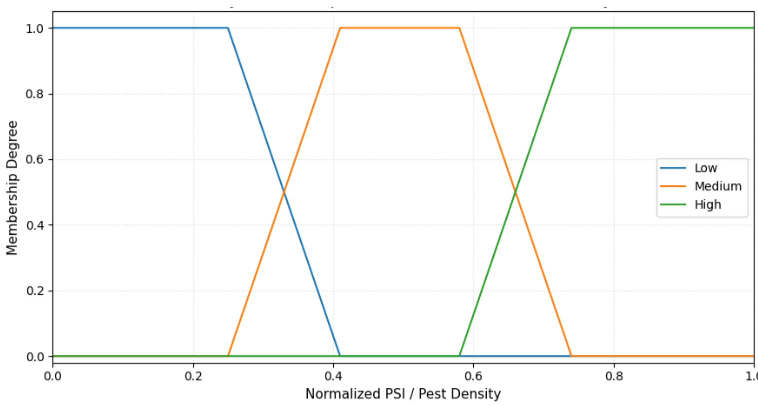

Figure 17. Overlapping trapezoidal membership functions defining the fuzzy linguistic levels low, medium, and high for the normalized Physiological Stress Index (PSI) and normalized pest-density indicator (PD).

Following fuzzification, all nine PSI–PD decision rules were evaluated using the minimum operator for fuzzy rule activation, and the recommendation associated with the dominant activated rule was selected as the final decision-support output (Table 10).

Table 10. Explainable rule-based decision logic.

PSI	Pest Density (PD)	Recommendation
Low	Low	Continue routine monitoring
Low	Medium	Increase observation frequency
Low	High	Inspect crop for localized infestation
Medium	Low	Inspect crop physiological condition
Medium	Medium	Increase monitoring and prepare preventive actions
Medium	High	Perform targeted field inspection
High	Low	Investigate water or environmental stress
High	Medium	Perform field inspection and preventive treatment
High	High	Immediate intervention recommended

The rule base summarized in Table 10 is graphically represented by the explainable decision matrix shown in Figure 18. The matrix illustrates how the combined physiological stress level and normalized pest-density level are translated into transparent agronomic recommendations. The decision intensity progressively increases from routine monitoring under low physiological stress and pest density to immediate intervention when both indicators simultaneously reach the highest risk category.

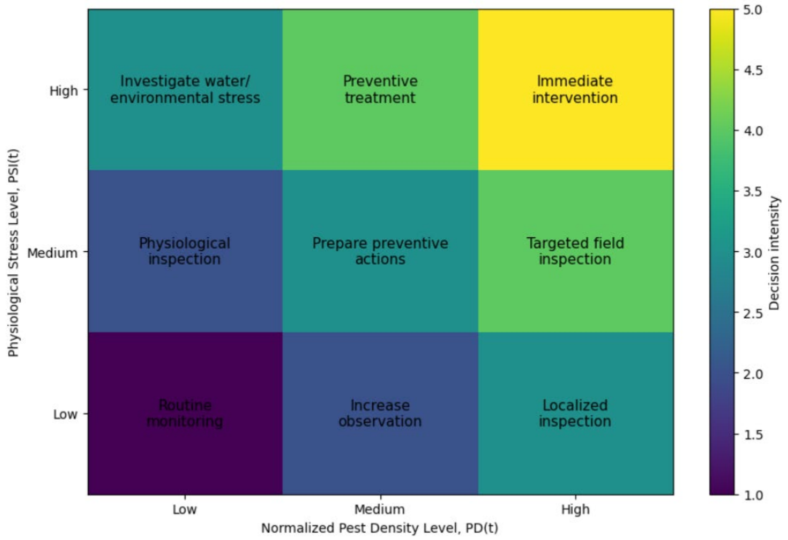

Figure 18. Explainable decision matrix integrating the Physiological Stress Index (PSI) and normalized pest-density indicator (PD). Each matrix element represents the agronomic recommendation generated by the proposed transparent rule-based decision-support system.

The proposed rule base is intentionally transparent, enabling every recommendation to be directly traced to the corresponding physiological stress and pest-density levels. Such interpretability is particularly important for smart agriculture applications, where agronomic decisions must remain understandable, verifiable, and consistent with expert knowledge. Unlike purely data-driven approaches, the proposed framework preserves explicit decision logic while integrating the predictive capability of machine learning.

Overall, the proposed explainable DSS combines physiological monitoring, embedded AI-based pest monitoring, short-term PSI prediction, fuzzy linguistic representation, and transparent rule-based reasoning within a unified framework suitable for edge-enabled precision agriculture. The modular architecture also enables the future incorporation of additional environmental variables, disease-risk indicators, weather forecasts, cloud-based analytics, and autonomous agricultural robots without fundamentally modifying the underlying explainable decision logic.

To demonstrate the predictive capability of the proposed framework beyond the available monitoring period, the Gradient Boosting model developed specifically for the 1 h forecasting horizon was integrated with the explainable rule base. Gradient Boosting was selected because it achieved the strongest predictive performance at the 1 h horizon (MAE = 0.0429, RMSE = 0.0616, R^2 = 0.9034). Following the final physiological observation recorded on 11 July 2026, recursive hourly PSI predictions were generated from the first subsequent 1 h forecasting step through the end of 13 July 2026. Only the two complete calendar days, 12 and 13 July 2026, were retained for daily aggregation and decision-support analysis. Because future environmental and physiological measurements were unavailable, the latest observed values of the exogenous predictors were held constant throughout the forecasting period, while the predicted PSI was recursively updated at each 1 h forecasting step. The latest available pest-density measurement acquired on 11 July 2026 was carried forward as the current pest-status indicator. The hourly PSI predictions were aggregated by day, and the mean predicted PSI was combined with the normalized pest-density indicator through the fuzzy rule-based inference mechanism. The corresponding fuzzy membership degrees were calculated for both inputs, all nine rules were evaluated using the minimum operator, and the dominant activated rule determined the final agronomic recommendation. The maximum predicted PSI was additionally reported as an indicator of within-day peak stress. The resulting predictive decision-support outputs are summarized in Table 11.

Table 11. Predictive fuzzy explainable decision-support results for the two-day forecast period.

Date	Mean PSI	Max PSI	PSI Level	Pest Density	Normalized PD	PD Level	Rule Activation	Recommendation
12 July 2026	0.551	0.551	Medium	37.2	0.593	Medium	0.919	Increase monitoring and prepare preventive actions
13 July 2026	0.5519	0.551	Medium	37.2	0.593	Medium	0.919	Increase monitoring and prepare preventive actions

The predictive decision-support results demonstrate the practical operation of the proposed fuzzy explainable decision-support system beyond the available physiological monitoring period. Under the adopted constant-input scenario, the recursively predicted PSI progressively converged toward approximately 0.551. The resulting mean and maximum daily PSI values were approximately 0.551 for both 12 and 13 July 2026, corresponding to dominant medium physiological-stress membership on both days. The latest available pest-density measurement (PD = 37.2; normalized PD = 0.593) exhibited dominant medium membership together with a smaller partial membership in the high category. For both forecast days, the medium–medium rule achieved the highest fuzzy activation (approximately 0.919), whereas the secondary medium–high rule showed substantially lower activation. Consequently, the dominant fuzzy rule generated the recommendation "Increase monitoring and prepare preventive actions" for both forecast days.

The gradual convergence of the predicted PSI toward a stable value reflects the adopted forecasting assumptions. Because the exogenous environmental and physiological predictors were maintained at their latest observed values while only the predicted PSI was recursively updated, the model progressively approached a steady-state response. Therefore, the similarity between the predicted values toward the end of the forecasting period should not be interpreted as evidence of unchanged real-world crop conditions, but rather as the expected behavior of the model under constant-input assumptions.

The generated recommendation indicates that the forecasted crop condition requires increased monitoring and timely preventive actions rather than immediate intervention. This example demonstrates the transparency of the proposed framework, since every recommendation can be directly traced to the fuzzy membership degrees of the predicted physiological-stress and pest-density indicators, the corresponding rule-activation strengths, and the dominant activated decision rule. Consequently, the proposed DSS combines the predictive capability of machine learning with explicit rule-based reasoning, providing recommendations that remain understandable, verifiable, and consistent with agronomic expertise.

The presented experiment represents a proof-of-concept implementation of the proposed predictive explainable decision-support methodology rather than an independently validated operational forecast. Because future environmental and physiological observations were unavailable, the latest measured exogenous predictor values were maintained throughout the forecasting period, while the predicted PSI was recursively propagated using the 1 h Gradient Boosting model. The resulting predictions should therefore be interpreted as a demonstration of the predictive decision-support workflow and the expected model response under unchanged external conditions. Future implementations could incorporate weather forecasts, dynamically updated physiological measurements, pest-population prediction, disease-risk indicators, adaptive PSI thresholds, and autonomous agricultural robots to enable fully dynamic and continuously updated decision support under real field conditions

4. Discussion

The proposed multimodal framework integrates environmental sensing, physiological monitoring, machine learning, and explainable decision support into a unified architecture for crop stress assessment. Unlike conventional approaches based on a single sensing modality, it combines atmospheric and physiological information, providing a more comprehensive evaluation of crop stress under changing environmental conditions. This concept is consistent with recent studies demonstrating that multimodal sensing improves the robustness and reliability of precision agriculture decision making [11,14,43–45].

As expected from its composite formulation, the strong correlations between the proposed Physiological Stress Index (PSI) and the principal environmental variables (VPD: r = 0.980; ΔT: r = 0.990; RH: r = -0.961) indicate that PSI closely reflects atmospheric conditions associated with plant water stress, consistent with previous studies [44,45]. Furthermore, the inclusion of leaf capacitance (CAP) and relative irradiance (IRR) provides complementary physiological information beyond environmental measurements alone, supporting the use of PSI as an interpretable stress indicator for subsequent machine-learning prediction and explainable decision support.

The machine-learning results showed that predictive performance depended on the forecasting horizon. At the 15 min horizon, Linear Regression and Gradient Boosting demonstrated virtually identical performance, with Gradient Boosting achieving marginally better RMSE and R^2 values. At the 30 min horizon, Linear Regression achieved marginally better RMSE and R^2 values, whereas Gradient Boosting provided the strongest overall performance from the 1 h horizon onward. These results suggest that both linear and nonlinear models effectively capture very short-term PSI dynamics, while nonlinear relationships become increasingly relevant as the forecasting horizon increases. These findings support the use of complementary regression approaches for short- and medium-term physiological stress forecasting and are consistent with recent agricultural studies and our previous work demonstrating the effectiveness of both linear and ensemble learning approaches for data-driven prediction [46–52]. The resulting predictive performance enabled predicted PSI values to be incorporated into the proposed explainable decision-support framework for short-term agronomic forecasting.

The proposed framework combines machine-learning prediction with an explainable rule-based decision-support system, where machine-learning predicts the future Physiological Stress Index, while transparent decision rules generate agronomic recommendations. This hybrid approach preserves both predictive capability and interpretability, supporting trustworthy decision making in precision agriculture [34–36]. The predictive DSS demonstration further showed that the forecasted PSI values can be directly translated into transparent management recommendations by combining the predicted physiological stress level with the latest available pest-density information. This integration enables short-term proactive decision support while maintaining full traceability of every recommendation.

Interpretable rule-based reasoning has been widely adopted across different application domains, including fuzzy logic systems [53] and hybrid expert systems, for agricultural decision support that transform expert knowledge into transparent recommendations [54–56]. The proposed framework follows the same principle by generating straightforward and easily interpretable agronomic recommendations while preserving complete transparency of the decision-making process.

Although fixed PSI thresholds were adopted to simplify implementation, adaptive threshold optimization represents a promising direction for future research. Future versions of the proposed framework may incorporate dynamically adjusted PSI thresholds derived from long-term field observations, weather forecasts, or machine-learning models while preserving the transparency and interpretability of the explainable decision-support process [34,45].

The predictive DSS presented in this study should be interpreted as a proof-of-concept demonstration of short-term forecasting. The two-day prediction scenario was generated immediately after the available monitoring period by recursively predicting PSI while maintaining the latest observed environmental and physiological conditions. Consequently, the generated recommendations represent a constant-input forecasting scenario rather than an independently validated long-term prediction. Nevertheless, the presented experiment demonstrates the practical integration of machine-learning prediction with transparent decision-support logic and illustrates how future physiological stress can be transformed into understandable agronomic recommendations.

Although the present study was conducted on pepper plants under specific field conditions, the proposed framework was designed as a modular sensing and decision-support architecture rather than as a crop-specific system. The experimental implementation was based on the commercial METOS/FieldClimate ecosystem, which supports modular integration of environmental, physiological, and pest-monitoring devices and has been deployed across diverse agricultural applications and environmental conditions. Consequently, the general system architecture can be transferred to other crops and sensor configurations without changing its fundamental data-acquisition and fusion structure. However, crop-dependent components, particularly PSI weighting parameters, stress thresholds, and agronomic decision rules, would require crop- and environment-specific recalibration and validation. Future multi-crop, multi-site, and multi-season experiments are therefore required to establish broader biological generalizability.

Overall, the proposed framework combines environmental sensing, physiological monitoring, AI-based pest detection, machine-learning prediction, and explainable decision support within a unified edge-enabled IoT architecture. By integrating mathematical modelling with data-driven intelligence, the framework enables transparent and proactive crop management, consistent with recent advances in precision agriculture [11,34] and hybrid intelligent systems [57]. Future research will focus on large-scale field validation across different crops and cultivable areas, integration of weather forecasts and dynamic pest-population prediction, adaptive PSI thresholds, as well as secure edge-enabled IoT infrastructures and autonomous robotic platforms to support reliable, resilient, and automated precision agriculture applications [58,59].

5. Conclusions

This study presented an edge-enabled multimodal agricultural intelligence framework integrating environmental sensing, wearable plant physiological monitoring, AI-based pest detection, machine-learning prediction, and explainable decision support for precision agriculture. The proposed PSI provided an interpretable indicator of crop physiological stress. The evaluated machine-learning models demonstrated reliable short-term PSI prediction, with Linear Regression and Gradient Boosting showing comparable performance at the shortest forecasting horizon and Gradient Boosting providing stronger performance at longer forecasting horizons. By integrating the machine-learning-predicted PSI with pest-density information through a transparent fuzzy rule-based decision-support system, the proposed framework enabled proactive, explainable, and traceable agronomic recommendations. The proof-of-concept predictive DSS demonstrated how machine-learning forecasts can be translated into practical crop-management actions while preserving full interpretability of the decision-making process. Future research will focus on multi-season field validation, integration of weather forecasts and dynamic pest-population prediction, adaptive PSI threshold optimization, and deployment on autonomous robotic platforms for precision agriculture. Overall, the proposed framework demonstrates the potential of combining multimodal sensing, machine learning, explainable artificial intelligence, and edge-enabled IoT technologies to support reliable, transparent, and intelligent precision agriculture.

Supplementary Materials: The following supporting information can be downloaded at https://www.mdpi.com/article/10.3390/electronics15173816/s1: Data S1: synchronized environmental and physiological dataset used for PSI computation and machine-learning analysis; Code S1: Python/Jupyter Notebook containing data preprocessing, synchronization, PSI computation, statistical analysis, machine-learning evaluation, multi-horizon prediction analysis, fuzzy rule-based decision-support analysis, and figure generation.

Author Contributions: Conceptualization, V.A.K.; methodology, V.A.K.; software, V.A.K.; validation, V.A.K.; formal analysis, V.A.K.; investigation, V.A.K. and V.J.; data curation, V.A.K.; writing—original draft preparation, V.A.K.; writing—review and editing, V.A.K. and V.J.; visualization, V.A.K.; supervision, V.A.K.; project administration, V.J. All authors have read and agreed to the published version of the manuscript.

Funding: This research was funded by the Ministry of Education and Science of the Republic of North Macedonia under the national research project "Mathematical Models in Machine Learning for Smart Agriculture and High-Value Food" (Project ID: 718489; Grant No. 15-6171/22, dated 7 August 2025).

Data Availability Statement: The synchronized dataset and analysis code supporting the results presented in this study are provided as Supplementary Materials. Additional information may be obtained from the corresponding author upon reasonable request.

Conflicts of Interest: The authors declare no conflicts of interest.

Abbreviations

The following abbreviations are used in this manuscript:

AI	Artificial Intelligence
CAP	Leaf Capacitance Response
CSV	Comma-Separated Values
DSS	Decision Support System
GB	Gradient Boosting
IoT	Internet of Things
IRR	Relative Irradiance
ML	Machine Learning
PD	Pest Density
PSI	Physiological Stress Index
RF	Random Forest
RH	Relative Humidity
ROI	Region of Interest
SM	Soil Moisture
VPD	Vapor Pressure Deficit
XAI	Explainable Artificial Intelligence

References

1. Mansoor, S.M.; Iqbal, S.S.; Popescu, S.M.; Kim, S.L.; Chung, Y.S.; Baek, J.-H. Integration of Smart Sensors and IoT in Precision Agriculture: Trends, Challenges and Future Prospectives. *Front. Plant Sci.* **2025**, *16*, 1587869. [CrossRef] [PubMed]
2. Sudha, S.P.; Shajilin Loret, J.B. A Review on Machine Learning-Based Precision Agriculture Techniques for Crop Farming Monitoring with IoT. *Discov. Environ.* **2026**, *4*, 10. [CrossRef]
3. Eze, V.H.U.; Eze, E.C.; Alaneme, G.U.; Bubu, P.E.; Nnadi, E.O.E.; Okon, M.B. Integrating IoT Sensors and Machine Learning for Sustainable Precision Agroecology: Enhancing Crop Resilience and Resource Efficiency through Data-Driven Strategies, Challenges, and Future Prospects. *Discov. Agric.* **2025**, *3*, 83. [CrossRef]
4. Rajbongshi, A.; Johora, F.T.; Hossain, A.; Sarker, M.S.; Rahman, M.H.; Rahman, M.W.; Alotaibi, F.T.; Moni, M.A. Leveraging Explainable AI for Sustainable Agriculture: A Comprehensive Review of Recent Advances. *Artif. Intell. Rev.* **2026**, *59*, 105. [CrossRef]
5. Sharma, K.; Bhatt, U.; Soni, V. Artificial Intelligence-Assisted Detection of Abiotic Stress in Agricultural Crops: Sensors, Computational Models, and Outlook. *J. Crop Health* **2026**, *78*, 71. [CrossRef]
6. Jawad, H.M.; Nordin, R.; Gharghan, S.K.; Jawad, A.M.; Ismail, M. Energy-Efficient Wireless Sensor Networks for Precision Agriculture: A Review. *Sensors* **2017**, *17*, 1781. [CrossRef]
7. Wolfert, S.; Ge, L.; Verdouw, C.; Bogaardt, M.-J. Big Data in Smart Farming—A Review. *Agric. Syst.* **2017**, *153*, 69–80. [CrossRef]
8. Ayaz, M.; Ammad-Uddin, M.; Sharif, Z.; Mansour, A.; Aggoune, E.-H.M. Internet-of-Things (IoT)-Based Smart Agriculture: Toward Making the Fields Talk. *IEEE Access* **2019**, *7*, 129551–129583. [CrossRef]
9. Khanna, A.; Kaur, S. Evolution of Internet of Things (IoT) and Its Significant Impact in the Field of Precision Agriculture. *Comput. Electron. Agric.* **2019**, *157*, 218–231. [CrossRef]
10. Benos, L.; Tagarakis, A.C.; Dolias, G.; Berruto, R.; Kateris, D.; Bochtis, D. Machine Learning in Agriculture: A Comprehensive Updated Review. *Sensors* **2021**, *21*, 3758. [CrossRef] [PubMed]
11. Soussi, A.; Zero, E.; Sacile, R.; Trinchero, D.; Fossa, M. Smart Sensors and Smart Data for Precision Agriculture: A Review. *Sensors* **2024**, *24*, 2647. [CrossRef] [PubMed]
12. Knights, V.A.; Petrovska, O.; Kljusurić, J.G. Nonlinear Dynamics and Machine Learning for Robotic Control Systems in IoT Applications. *Future Internet* **2024**, *16*, 435. [CrossRef]
13. Manono, B.O.; Mwami, B.; Mutavi, S.; Nzilu, F. Precision Farming with Smart Sensors: Current State, Challenges and Future Outlook. *Sensors* **2026**, *26*, 882. [CrossRef]
14. Lakshmi, T.R.; Ambaru, B. The Biophysics of Precision Agriculture: Smart Sensors and Materials for Sustainable Farming: A Review. *Agric. Rev.* **2026**, *47*, 248–257. [CrossRef]
15. Kuunya, R.; Mohammed, E.A.H.; Osman, M.M.A.; Ssemugenze, B.; Tamás, A.; Ragán, P. Leveraging Remote Sensing Technologies: A Review of Precision Cropping Challenges and Research Trend Analysis. *J. Indian Soc. Remote Sens.* **2026**, *54*, 3399–3420. [CrossRef]
16. Ojha, T.; Misra, S.; Raghuwanshi, N.S. Wireless Sensor Networks for Agriculture: The State-of-the-Art in Practice and Future Challenges. *Comput. Electron. Agric.* **2015**, *118*, 66–84. [CrossRef]
17. Liakos, K.G.; Busato, P.; Moshou, D.; Pearson, S.; Bochtis, D. Machine Learning in Agriculture: A Review. *Sensors* **2018**, *18*, 2674. [CrossRef] [PubMed]
18. Ke, X.; Jiang, Z.; Qiao, A.; Yao, J.; Gu, X.; Ying, Z.; Zheng, Y.; Xu, K.; Zhou, Y.; Lu, C.; et al. A Shift From Environment- to Plant-Based Irrigation: Wearable Sensors Enabling Next-Generation Feedback Control. *Food Energy Secur.* **2026**, *15*, e70240. [CrossRef]
19. Pascoal, D.; Silva, N.; Adão, T.; Lopes, R.D.; Peres, E.; Morais, R. A Technical Survey on Practical Applications and Guidelines for IoT Sensors in Precision Agriculture and Viticulture. *Sci. Rep.* **2024**, *14*, 29793. [CrossRef]
20. Getahun, S.; Kefale, H.; Gelaye, Y. Application of Precision Agriculture Technologies for Sustainable Crop Production and Environmental Sustainability: A Systematic Review. *Sci. World J.* **2024**, *2024*, 2126734. [CrossRef]
21. Abou Samra, R.M.; Ali, R.R. Explainable Artificial Intelligence in Smart Agriculture: A Comprehensive Review of Interpretable Remote Sensing for Sustainable Decision-Making. *AgriEngineering* **2026**, *8*, 270. [CrossRef]
22. Nassar, J.M.; Khan, S.M.; Villalva, D.R.; Nour, M.M.; Almuslem, A.S.; Hussain, M.M. Compliant plant wearables for localized microclimate and plant growth monitoring. *npj Flex. Electron.* **2018**, *2*, 24. [CrossRef]
23. Lo Presti, D.; Cimini, S.; Massaroni, C.; D'Amato, R.; Caponero, M.A.; De Gara, L.; Schena, E. Plant Wearable Sensors Based on FBG Technology for Growth and Microclimate Monitoring. *Sensors* **2021**, *21*, 6327. [CrossRef]
24. Yan, X.; Pang, Y.; Niu, K.; Hu, B.; Zhu, Z.; Tan, Z.; Lei, H. Wearable Sensors for Plants: Status and Prospects. *Biosensors* **2025**, *15*, 53. [CrossRef]
25. Yan, B.; Zhang, F.; Wang, M.; Zhang, Y.; Fu, S. Flexible Wearable Sensors for Crop Monitoring: A Review. *Front. Plant Sci.* **2024**, *15*, 1406074. [CrossRef]

26. Ljubičić, N.; Figueredo, F.; Miler, I.; Sousa, L.R.; Barošević, T.; Tuccillo, M.; Buđen, M.; Stevanović, N.; Stanković, N.; Gimenez, V.D.; et al. On-Site Devices for Precision Agriculture Applications: A Review of Soil and Plant Sensors. *Agriculture* **2026**, *16*, 883. [CrossRef]
27. Valdiviezo, J.; Turpo, E.; Gutierrez, R.R.; Jaramillo-Carrión, M.; Aguilar-Lome, J.; Ruiz, L.A.; Ramos-Fernández, L. Remote Sensing and Artificial Intelligence for Crop Pest and Disease Monitoring: A Systematic Review of Sensing Technologies, AI Approaches, and Barriers to Field Adoption. *Smart Agric. Technol.* **2026**, *14*, 102279. [CrossRef]
28. Partel, V.; Nunes, L.; Stansly, P.; Ampatzidis, Y. Automated Vision-Based System for Monitoring Asian Citrus Psyllid in Citrus Groves. *Comput. Electron. Agric.* **2019**, *162*, 328–336. [CrossRef]
29. Alogla, A.A.; Baumers, M.; Tuck, C.; Elmadih, W. The Impact of Additive Manufacturing on the Flexibility of a Manufacturing Supply Chain. *Appl. Sci.* **2021**, *11*, 3707. [CrossRef]
30. Chen, K.; Yuan, Y.; Zhao, B.; Zhou, L.; Niu, K.; Jin, X.; Gao, S.; Li, R.; Guo, H.; Zheng, Y. Digital Twins and Data-Driven in Plant Factory: An Online Monitoring Method for Vibration Evaluation and Transplanting Quality Analysis. *Agriculture* **2023**, *13*, 1165. [CrossRef]
31. Sun, J.; Wang, Q.; Li, Q.; Xu, G.; Liang, B.; Ma, C.; Tian, S.; Gao, Q. Artificial Intelligence in Smart Agriculture Across the Production-to-Postharvest Continuum: Progress, Challenges, and Future Directions. *Sustainability* **2026**, *18*, 4908. [CrossRef]
32. Wu, Y.; Chen, L.; Yang, N.; Sun, Z. Research Progress of Deep Learning-Based Artificial Intelligence Technology in Pest and Disease Detection and Control. *Agriculture* **2025**, *15*, 2077. [CrossRef]
33. Javed, K.; Smagghe, G.; Wang, Q.; Javed, H.; Wang, Y. Artificial Intelligence in Crop Protection: Revolutionizing Agriculture for a Sustainable Future. *Inf. Process. Agric.* 2025; *in press*. [CrossRef]
34. Knights, V.A.; Prchkovska, M.; Krašnjak, L.; Kljusurić, J.G. Uncertainty-Aware Multimodal Fusion and Bayesian Decision-Making for DSS. *AppliedMath* **2026**, *6*, 16. [CrossRef]
35. Barredo Arrieta, A.; Díaz-Rodríguez, N.; Del Ser, J.; Bennetot, A.; Tabik, S.; Barbado, A.; García, S.; Gil-López, S.; Molina, D.; Benjamins, R.; et al. Explainable Artificial Intelligence (XAI): Concepts, Taxonomies, Opportunities and Challenges toward Responsible AI. *Inf. Fusion* **2020**, *58*, 82–115. [CrossRef]
36. Holzinger, A.; Langs, G.; Denk, H.; Zatloukal, K.; Müller, H. Causability and Explainability of Artificial Intelligence in Medicine. *WIREs Data Min. Knowl. Discov.* **2019**, *9*, e1312. [CrossRef]
37. Ortigossa, E.S.; Gonçalves, T.; Nonato, L.G. Explainable Artificial Intelligence (XAI)—From Theory to Methods and Applications. *IEEE Access* **2024**, *12*, 80799–80846. [CrossRef]
38. Kostopoulos, G.; Davrazos, G.; Kotsiantis, S. Explainable Artificial Intelligence-Based Decision Support Systems: A Recent Review. *Electronics* **2024**, *13*, 2842. [CrossRef]
39. Jackson, R.D.; Idso, S.B.; Reginato, R.J.; Pinter, P.J., Jr. Canopy Temperature as a Crop Water Stress Indicator. *Water Resour. Res.* **1981**, *17*, 1133–1138. [CrossRef]
40. Dwivedi, A.K.; Ojha, C.S.P.; Singh, V.P. Crop Water Stress Index for Scheduling Irrigation of Wheat Crop. *J. Irrig. Drain. Eng.* **2024**, *150*, 04024006. [CrossRef]
41. Sun, T.; Lu, C.; Shi, Z.; Zou, M.; Bi, P.; Xu, X.; Xie, Q.; Jiang, R.; Liu, Y.; Cheng, R.; et al. PlantRing: A High-Throughput Wearable Sensor System for Decoding Plant Growth, Water Relations, and Innovating Irrigation. *Plant Commun.* **2025**, *6*, 101322. [CrossRef]
42. Hoh, D.; Suh, H.K.; Kaiser, E. Let's Get Real: Are Wearable Plant Sensors Ready for Crop Monitoring? *ACS Sens.* **2025**, *10*, 8156–8169. [CrossRef]
43. Karmakar, P.; Teng, S.W.; Murshed, M.; Pang, S.; Li, Y.; Lin, H. Crop Monitoring by Multimodal Remote Sensing: A Review. *Remote Sens. Appl. Soc. Environ.* **2024**, *33*, 101093. [CrossRef]
44. Chakhvashvili, E.; Machwitz, M.; Antala, M.; Rozenstein, O.; Prikaziuk, E.; Schlerf, M.; Naethe, P.; Wan, Q.; Komárek, J.; Klouek, T.; et al. Crop Stress Detection from UAVs: Best Practices and Lessons Learned for Exploiting Sensor Synergies. *Precis. Agric.* **2024**, *25*, 2614–2642. [CrossRef]
45. Cho, S.B.; Soleh, H.M.; Choi, J.W.; Hwang, W.-H.; Lee, H.; Cho, Y.-S.; Cho, B.-K.; Kim, M.S.; Baek, I.; Kim, G. Recent Methods for Evaluating Crop Water Stress Using AI Techniques: A Review. *Sensors* **2024**, *24*, 6313. [CrossRef]
46. Mahesh, P.; Soundrapandiyan, R. Yield Prediction for Crops by Gradient-Based Algorithms. *PLoS ONE* **2024**, *19*, e0291928. [CrossRef]
47. Parganiha, V.; Verma, M. An Effective Soil Analysis and Crop Yield Prediction Based on Optimised LightGBM in Smart Agriculture. *J. Agron. Crop Sci.* **2024**, *210*, e12726. [CrossRef]
48. Pukrongta, N.; Taparugssanagorn, A.; Sangpradit, K. Enhancing Crop Yield Predictions with PEnsemble 4: IoT and ML-Driven for Precision Agriculture. *Appl. Sci.* **2024**, *14*, 3313. [CrossRef]
49. Sharma, R.; Kaur, J.; Feng, G.; Huang, Y.; Kumar, C.; Wang, Y.; Sharma, S.; Jenkins, J.; Dhillon, J. Maize and Soybean Yield Prediction Using Machine Learning Methods: A Systematic Literature Review. *Discov. Agric.* **2025**, *3*, 64. [CrossRef]

50. Choi, J.W.; Hidayat, M.S.; Cho, S.B.; Hwang, W.-H.; Lee, H.; Cho, B.-K.; Kim, M.S.; Baek, I.; Kim, G. Recent Trends in Machine Learning, Deep Learning, Ensemble Learning, and Explainable Artificial Intelligence Techniques for Evaluating Crop Yields under Abnormal Climate Conditions. *Plants* **2025**, *14*, 2841. [CrossRef]
51. Knights, V.A.; Petrovska, O.; Prchkovska, M. Machine Learning and Mathematical Modeling in Agricultural Development. In *International Conference on Intelligence-Based Transformations of Technology and Business Trends*; Springer Nature: Cham, Switzerland, 2025; pp. 249–262.
52. Knights, V.; Prchkovska, M. From Equations to Predictions: Understanding the Mathematics and Machine Learning of Multiple Linear Regression. *J. Math. Comput. Appl.* **2024**, *3*, 137. [CrossRef]
53. Knights, V.A.; Gacovski, Z. Fuzzy Rule-Based System as a Method of Modeling for Estimation Quality of the Vardar River. *Am. Acad. Sci. Res. J. Eng. Technol. Sci.* **2023**, *91*, 105–112. Available online: https://asrjetsjournal.org/American_Scientific_Journal/article/view/8607 (accessed on 17 July 2026).
54. Papadopoulos, A.; Kalivas, D.; Hatzichristos, T. Decision Support System for Nitrogen Fertilization Using Fuzzy Theory. *Comput. Electron. Agric.* **2011**, *78*, 130–139. [CrossRef]
55. Prabakaran, G.; Vaithiyanathan, D.; Ganesan, M. Fuzzy Decision Support System for Improving the Crop Productivity and Efficient Use of Fertilizers. *Comput. Electron. Agric.* **2018**, *150*, 88–97. [CrossRef]
56. Rupnik, R.; Kukar, M.; Vračar, P.; Košir, D.; Pevec, D.; Bosnić, Z. AgroDSS: A Decision Support System for Agriculture and Farming. *Comput. Electron. Agric.* **2019**, *161*, 260–271. [CrossRef]
57. Knights, V.A.; Petrovska, O.; Kljusurić, J.G. Symmetry and Asymmetry in Dynamic Modeling and Nonlinear Control of a Mobile Robot. *Symmetry* **2025**, *17*, 1488. [CrossRef]
58. Antoska Knights, V.; Gacovski, Z. Methods for Detection and Prevention of Vulnerabilities in the IoT (Internet of Things) Systems [Internet]. In *Internet of Things—New Insights*; IntechOpen: London, UK, 2024. [CrossRef]
59. Knights, V.A.; Stankovski, M.; Nusev, S.; Temeljkovski, D.; Petrovska, O. Robots for Safety and Health at Work. *Mech. Eng. Sci. J.* **2015**, *33*, 275–279. Available online: https://www.mesj.ukim.edu.mk/journals/issue/download/17/9 (accessed on 15 July 2026).